Role of TOMM34 on NF-κB activation-related hyperinflammation in severely ill patients with COVID-19 and influenza

Qiwen Shi,[b,d] Pengfei Zhang,[c,d] Qingtao Hu,[a,d] Tianxin Zhang,[c,d] Ruixia Hou,[b] Shengxiang Yin,[c] Yilin Zou,[c] Fenghua Chen,[a] Shuang Jiao,[c] Lanlan Si,[a] Bangjin Zheng,[c] Yichao Chen,[c] Tingzhu Zhan,[b] Yongxiang Liu,[c,*] Wenting Zhu,[c,**] and Nan Qi[a,c,***]

[a]State Key Laboratory of Respiratory Disease, The First Affiliated Hospital of Guangzhou Medical University, Guangzhou, 510120, China
[b]Collaborative Innovation Center of Yangtze River Delta Region Green Pharmaceuticals, College of Pharmaceutical Sciences, Zhejiang University of Technology, Hangzhou, 310014, China
[c]Guangzhou National Laboratory, Guangzhou International Bio-Island, Guangzhou, 510005, China

Summary

Background Highly pathogenic respiratory RNA viruses such as SARS-CoV-2 and its associated syndrome COVID-19 pose a tremendous threat to the global public health. Innate immune responses to SARS-CoV-2 depend mainly upon the NF-κB-mediated inflammation. Identifying unknown host factors driving the NF-κB activation and inflammation is crucial for the development of immune intervention strategies.

Methods Published single-cell RNA sequencing (scRNA-seq) data was used to analyze the differential transcriptome profiles of bronchoalveolar lavage (BAL) cells between healthy individuals ($n = 27$) and patients with severe COVID-19 ($n = 21$), as well as the differential transcriptome profiles of peripheral blood mononuclear cells (PBMCs) between healthy individuals ($n = 22$) and severely ill patients with COVID-19 ($n = 45$) or influenza ($n = 16$). Loss-of-function and gain-of-function assays were performed in diverse viruses-infected cells and male mice models to identify the role of TOMM34 in antiviral innate immunity.

Findings *TOMM34*, together with a list of genes encoding pro-inflammatory cytokines and antiviral immune proteins, was transcriptionally upregulated in circulating monocytes, lung epithelium and innate immune cells from individuals with severe COVID-19 or influenza. Deficiency of TOMM34/Tomm34 significantly impaired the type I interferon responses and NF-κB-mediated inflammation in various human/murine cell lines, murine bone marrow-derived macrophages (BMDMs) and *in vivo*. Mechanistically, TOMM34 recruits TRAF6 to facilitate the K63-linked polyubiquitination of NEMO upon viral infection, thus promoting the downstream NF-κB activation.

Interpretation In this study, viral induction of TOMM34 is positively correlated with the hyperinflammation in severely ill patients with COVID-19 and influenza. Our findings also highlight the physiological role of TOMM34 in the innate antiviral signallings.

Funding A full list of funding sources can be found in the acknowledgements section.

Keywords: COVID-19; Innate immunity; Inflammation; NF-κB; TOMM34

Introduction

In the last two decades, global public health has been facing a grave challenge from three highly pathogenic coronaviruses and their associated syndromes: severe acute respiratory syndrome (SARS) in 2002, Middle East respiratory syndrome (MERS) in 2012, and the coronavirus disease 2019 (COVID-19) that takes away millions of human lives. As most RNA virus, the COVID-19 causative agent SARS Coronavirus 2 (SARS-CoV-2) constantly mutates to generate circulating variants of

*Corresponding author.
**Corresponding author.
***Corresponding author.State Key Laboratory of Respiratory Disease, The First Affiliated Hospital of Guangzhou Medical University, Guangzhou 510120, China.
E-mail addresses: liu_yongxiang@gzlab.ac.cn (Y. Liu), zhu_wenting@gzlab.ac.cn (W. Zhu), qi_nan@gzlab.ac.cn (N. Qi).
[d]Contributed equally.

Research in context

Evidence before this study

COVID-19, caused by SARS-CoV-2, has taken away millions of human life worldwide in the past four years. Although WHO announced that COVID-19 no longer constitutes a Public Health Emergency of International Concern on May 5th 2023, we are still facing continuous threats from circulating variants of SARS-CoV-2 such as Omicron JN.1, as well as from other endemic respiratory RNA viruses such as Influenza A virus (IAV) and Respiratory syncytial virus (RSV). Severely ill patients with COVID-19 often undergo the respiratory distress syndrome (ARDS), and long-termly suffer from the post-acute COVID-19 syndrome (PACS) even after recovery, in which the virus-triggered inflammation plays a key role. Therefore, fundamental understanding of the antiviral signal transduction driving inflammation is critical for developing immune therapeutic intervention strategies.

Added value of this study

This work supported by the clinical, physiological and mechanistic data: (i) establish a correlation between viral induction of TOMM34 and the hyperinflammatory state in severely ill patients with COVID-19 and influenza; (ii) highlight the physiological significance of TOMM34 in the innate immune responses to RNA viruses; (iii) characterise the TRAF6-TOMM34-NEMO axis that is pivotal for the activation of NF-κB.

Implications of all the available evidence

TOMM34 is suggested to function as a double-edged sword in innate immunity: During the early phase of viral infection, the presence of TOMM34 ensures that the antiviral innate immune signalling is well facilitated to eliminate viruses; the induction of TOMM34 promotes the overactivation of NF-κB and excessive production of pro-inflammatory cytokines/chemokines, resulting in the cytokine storm syndrome at the late stage of diseases. Our studies thus establish TOMM34 as a valuable candidate protein for further investigation as an immune therapeutic target against viral infectious diseases and following inflammatory syndromes.

concern (VOCs) such as Omicron JN.1, thus eluding the current vaccines and treatments. Notably, SARS-CoV-2 and its low pathogenic counterparts (human endemic coronaviruses HCoV-OC43/NL63/229E, etc.) often activate shared cellular pathways and exploit common processes in their life cycles. Therefore, the host proteins involved in viral immunopathogenesis are potential targets of antivirals with a broad-spectrum activity against coronaviruses.

Innate immunity acts as the first line of host defense against viruses. Following the cell entry by surface receptors, respiratory RNA viruses such as SARS-CoV-2, IAV and RSV release their genomic RNA that activate the cytosolic RNA sensors RIG-I and MDA5.[1–5] MAVS (also called VISA, IPS-1 or Cardif), an adaptor protein located at mitochondria, is subsequently triggered by RIG-I/MDA5 to aggregate and form a signalsome with multiple ubiquitin E3 ligases TRAF2/5/3/6, leading to the downstream activation and nuclear translocation of two master transcription factors NF-κB and IRF3.[6–9] In the nucleus, the transcription of pro-inflammatory cytokines and chemokines (TNF-α, IL-1β, IL-6, IL-18, RANTES/CCL5, IP-10/CXCL10, MCP-1/CCL2, etc.) are stimulated by NF-κB, while type I interferons (IFN-α/β) are expressed under the collaboration of NF-κB and IRF3.[10–12] Inflammatory responses such as the NLRP3 inflammasome-mediated cell death pyroptosis, together with the effects of numerous IFN-stimulated genes (ISGs) are eventually induced to establish a robust antiviral state.[13] It should be noticed that the spike and envelope protein of beta-coronaviruses can activate the membrane toll-like receptor TLR4-/TLR2-related signalling in macrophages, respectively, thereby inducing the pro-inflammatory cytokines expression.[14,15] However, innate immune response is a double-edged sword in the host-virus arms race. Excessive activation of antiviral signalling and dysregulated release of inflammatory agents (e.g., IL-6, TNF-α, and CCL2) could result in the cytokine storm syndrome (CSS), a hallmark of severely ill patients with COVID-19 and other infectious diseases.[16] Growing evidences show that the SARS-CoV-2-infected monocytes and tissue-resident macrophages undergo inflammasome activation together with pyroptosis, which mainly contributes to the systemic hyperinflammation in COVID-19 pathogenesis.[17,18] Even after recovery, a considerable number of severely ill patients with COVID-19 indeed suffer from chronic sustained inflammation, which might be attributed to the IL-6-driving epigenetic memory in circulating hematopoietic stem and progenitor cells (HSPCs) and their progeny myeloid cells.[19] For developing the immune intervention strategies, it is imperative to fundamentally understand the antiviral signal transduction driving the NF-κB activation and downstream inflammatory responses.

IκB kinase gamma (IKKγ) is a key regulatory subunit of the IKK complex (IKKα/β/γ) responsible for the NF-κB activation, and thus is also designated as NF-κB essential modulator (NEMO). Upon stimulation with viruses or lipopolysaccharide (LPS), NEMO is conjugated to the K63-linked ubiquitin chains by E3 ligase TRAF6, allowing TAK1 to phosphorylate and activate the catalytic subunits IKKα/β.[20] The IKK complex then promotes the ubiquitin-proteasome degradation of IκBα, which releases NF-κB and facilitates its nuclear translocation for the further transcription of target genes related to immune responses.[21] Lacking of NEMO

disrupts the activation of IKK complex and NF-κB *in vivo* and in cells under certain stimulation.[22–24] Owing to its physiological significance in the antiviral immune signalling, NEMO has emerged as an ideal target of virus for countering the host innate immunity. Our group previously demonstrated that SARS-CoV-2 ORF9b antagonises the antiviral IFN and NF-κB signallings by interrupting the K63-linked ubiquitination of NEMO.[1] Besides, SARS-CoV-2 3CLpro can cleave NEMO to suppress the innate immune response.[25] NEMO was also reported as the cleavage substrate of Hepatitis A virus 3C protease to dampen the IFN-β induction.[26] Muscolino et al. revealed that Herpesvirus induces the autophagic degradation of NEMO for its immune evasion.[27] However, little is known about the host proteins which positively regulate the activation of NEMO and downstream signalling.

Mitochondria provide a platform for the antiviral signal transduction and host-virus interplay. A considerable amount of innate immune signalling components/regulators such as MAVS, NLRX1, USP18 and MFN1, are located at mitochondria and hijacked by viruses for immune evasion.[28–31] Translocase of the outer mitochondrial membrane (TOMM) is a multimeric protein complex accountable for initial recognition and import of mitochondrial preproteins from the cytosol.[32,33] Members of the TOMM family such as TOMM6, TOMM20, TOMM34, TOMM40 and TOMM70, were previously found to be associated with the Hsp70/Hsp90 chaperone complex, cancer progression, immune regulation and other processes.[34–39] TOMM70 is the first TOMM protein identified as an innate immune regulator by linking MAVS to the TBK1/IRF3 signalling cascade.[40] Recently, TOMM70 was reported to be sequestered by SARS-CoV-2 ORF9b for viral evasion of the IFN antiviral response.[41,42] In addition to TOMM70, whether other TOMM proteins are involved in antiviral innate immunity remains to be elucidated. In this study, we analyzed the differential transcriptome profiles of BAL cells and PBMCs from healthy individuals and patients infected by SARS-CoV-2 or PBMCs from healthy individuals and patients infected by influenza viruses. We uncovered a positive correlation between the viral induction of TOMM34 and the elevation of pro-inflammatory cytokines/chemokines in severely ill patients with COVID-19 or influenza. Using infected cells and mice models, we further revealed a distinct role of TOMM34 from TOMM70 in facilitating the innate immune responses to diverse RNA viruses, and finally dissected the underlying mechanism. Our study thus identifies TOMM34 as a key signalling modulator of antiviral innate immunity, and provides fundamental insights into the aberrant expression of inflammatory agents in severely ill patients with COVID-19 and other viral infectious diseases.

Methods

Cell cultures and viral strains

A549-ACE2 (A549 cells stably expressing ACE2), Caco-2-N (Caco-2 cells stably expressing SARS-CoV-2 nucleocapsid protein),[43] THP-1, HEK293T, A549, HeLa, NIH/3T3 cell lines were cultured in DMEM or RPMI 1640 (Thermo Fisher Scientific, USA) supplemented with 10% fetal bovine serum (FBS; Thermo Fisher Scientific, USA) and 1% penicillin-streptomycin (solarbio, China). All cells were mycoplasma-free and incubated at 37 °C in a 5% CO_2 humidified atmosphere. Cells were transiently transfected with respective plasmids or poly(I:C) using lipofectamine 3000 (Thermo Fisher Scientific, USA) or Hieff Trans™ Liposomal Transfection Reagent (Yeasen Biotechnology, China) according to the manufacturers' instructions. The resources of cell lines and reagents used in this work can be found in Supplementary Table S1.

The SARS-CoV-2 strain 2019-nCoV WIV04 was isolated from the BAL of a confirmed patient with COVID-19 by inoculating onto Vero E6 cells.[44] The transcription and replication-competent SARS-CoV-2 virus-like-particles (SARS-CoV-2 trVLP), which can be manipulated in a BSL-2 laboratory,[43] was a kind gift from Prof. Qiang Ding (Tsinghua University). The IAV strain A/Puerto Rico/8/1934 (H1N1; PR8) and its recombinant virus PR8-GFP were generously gifted from Dr. Shaobo Wang (Guangzhou National Laboratory) and Prof. Rui-kun Du (Shandong University of Traditional Chinese Medicine, using the same construction strategy as described[45]), respectively. The RSV strain A-0594 was obtained from Dr. Martin Ludlow (University of Veterinary Medicine Hannover); while Sendai virus (SeV, Cantell strain), vesicular stomatitis virus (VSV) and its recombinant virus VSV-DM51-GFP were obtained from Dr. Lei-Ke Zhang (Wuhan Institute of Virology, Chinese Academy of Sciences). See also Supplementary Table S1.

Mice

Lyz2-Cre mice on the C57BL/6 background were purchased from Shanghai Research Center for Model Organisms. *Tomm34*^{fl/fl} mice were generated using the CRISPR-Cas9 system and constructed by Shanghai Research Center for Model Organisms. Two loxP sequences were inserted in the introns flanked with the exon 2 of *Tomm34*. *Tomm34*^{fl/fl} *Lyz2-Cre* mice were generated by crossing the *Lyz2-Cre* mice with *Tomm34*^{fl/fl} mice for specific deletion of Tomm34 in myeloid cells. All mice were kept and bred in a specific pathogen-free (SPF) facility at Zhejiang University of Technology with a 12 h light/12 h dark cycle. All animal experiments were undertaken in accordance with the National Institute of Health Guide for the Care and Use of Laboratory Animals with approval of the Animal Care and Use Committee at Zhejiang University of Technology.

Plasmids

Human complementary DNA was amplified from total RNA extracted from HEK293T cells using HyperScript III 1st Strand cDNA Synthesis Kit (EnzyArtisan). Full-length *TOMM6*, *TOMM20*, *TOMM34*, *TOMM40*, *TOMM70* and *TRAF6* were cloned from Human cDNA and then inserted into pcDNA3.1-HA expression vector. HA-ubiquitin-WT, K63, K48 were gifted from Prof. Di Wang (Zhejiang University School of Medicine). HA-ubiquitin-K63R and K48R were purchased from Miaoling Biotechnology (China). The Flag-tagged RIG-I, MAVS, TBK1, IRF3, IKK-β, and NEMO expression plasmids have been described previously.[1] The HA-tagged TOMM34 constructs, including TOMM34-Δ1-GFP, TOMM34-Δ2-GFP, TOMM34-Δ3-GFP, TOMM34(S93/16A), were generated from full length TOMM34 using overlapping PCR or recombinant cloning kit. All constructs were confirmed by DNA sequencing. Primers used in this study are listed in Supplementary Table S2.

Virus infection

Cells were seeded in 12-well plates at a density of 4×10^5 cells/well, and were incubated with SARS-CoV-2 (multiplicity of infection, MOI = 0.4), SARS-CoV-2 trVLP (MOI = 0.1), PR8/PR8-GFP (MOI = 1), RSV (MOI = 1), VSV/VSV-DM51-GFP (MOI = 0.1), or SeV (20 HA units/mL) for the indicated hours. For mice infection, age-matched male $Tomm34^{fl/fl}$ and $Tomm34^{fl/fl}$ *Lyz2-Cre* littermates were intraperitoneally injected with VSV (1×10^8 PFU per mouse) or infected with PR8 (50 PFU per mouse) by intranasal administration, respectively. Male mice were used since sex differences in the innate antiviral responses measured are negligible in this study. The weight and the survival of animals were monitored daily. After VSV infection for 24 h, the mice were euthanized by CO_2 and the lungs, spleens, livers and sera were collected; while the lungs and BAL were collected at 72 h after PR8 infection.

Plaque assay

The tissue homogenates from infected $Tomm34^{fl/fl}$ and $Tomm34^{fl/fl}$ *Lyz2-Cre* mice were used to infect monolayers of Vero cells. 1 h later, the homogenates were removed, and infected Vero cells were washed with PBS followed by incubation with DMEM containing 2% methylcellulose for 48 h. The cells were fixed with 4% paraformaldehyde for 15 min and stained with 1% crystal violet for 30 min before counting the plaques.

Immunofluorescence microscopy

For examining VSV and PR8 proliferation, cells were infected with VSV-GFP or PR8-GFP. At the indicated time after infection, fluorescence images were taken by OLYMPUS CKX53 microscope.

For determining the cellular localization of TOMM34, HeLa cells were transfected with HA-TOMM34 for 24 h, and were then mock-infected or infected with SeV for 12 h. Cells were then incubated with 200 nM Mito Tracker Red (Thermo Fisher Scientific). For cellular colocalization of TOMM34 with NEMO, HeLa cells were transfected with plasmid expressing HA-TOMM34 and Flag-NEMO for 24 h. After being washed with PBS and fixed by 4% paraformaldehyde, cells were permeabilised by 0.2% Triton X-100 and then labeled with DAPI for 5 min. Fluorescence images were taken by ZEISS LSM 800 confocol microscope.

For detecting the translocation of NF-κB/p65, $Tomm34^{-/-}$ and wild type NIH/3T3 cells were seeded on coverslips in a 24-well dish. SeV-infected group cells were infected with SeV (20 HA units/mL) for 12 h. After being washed with PBS and fixed by 4% paraformaldehyde, cells were stained with anti-p65 antibody (1:50) and Alexa Fluor 488 Conjugated secondary antibody (1:150). Nucleus was labeled with DAPI for 5 min. Fluorescence images were taken by OLYMPUS FV3000 confocol microscope.

Immunoprecipitations and immunoblotting analysis

Constructs were transfected into HEK293T cells for 36 h with or without VSV infection. After transfection, cells were harvested and lysed in RIPA lysis buffer (Beyotime, China). After a brief centrifugation, the lysates were immunoprecipitated with anti-HA agarose beads, anti-Flag agarose beads or protein A/G beads with indicated antibodies at 4 °C overnight, and the precipitants were washed three times with lysis buffer at 4 °C. The extract-bead mixture was then resuspended in SDS loading buffer. The precipitants or whole cell lysates were fractionated by SDS-PAGE and transferred to a PVDF membrane. Subsequent immunoblotting analysis was performed with indicated antibodies.

Generation of *TOMM34* knockout cell lines

HEK293T $TOMM34^{-/-}$, A549 $TOMM34^{-/-}$ and NIH/3T3 $Tomm34^{-/-}$ cell lines were generated using the CRISPR/Cas9 system.[46] Briefly, the guide RNA sequences were cloned into CRISPR/Cas9-based vectors which are puromycin-resistant. Then, the vectors were transfected into HEK293T cells, A549 cells and NIH/3T3 cells by lipofectamine 3000. After puromycin selection, single colonies were picked and verified by genome sequencing and immunoblotting. Oligonucleotides are listed in Supplementary Table S2.

RNA interfering

All siRNA duplexes were obtained from RIBOBIO Co., Ltd. (China). In brief, HEK293T cells were seeded in 12-well plates and transfected with siRNA duplexes using lipofectamine 3000. At 36 h post transfection, cells were collected for the following assays. Oligonucleotides are listed in Supplementary Table S2.

Dual-luciferase reporter assays

HEK293T cells were seeded in 12-well plates and transfected with TOMM34 expressing vector or empty vector (EV), together with 100 ng luciferase reporter plasmid and 20 ng Renilla luciferase plasmid pRL-TK. At 24 h post-transfection, cells were transfected with 2 mg/mL poly(I:C), or infected with VSV for 12 h. Following the manufacturer's instructions for Dual-Luciferase reporter gene assay kit (Yeasen Biotechnology, China), cell lysates were obtained to measure the luciferase activity by BioTek Synergy H1.

Quantitative real-time PCR

Total RNA was extracted from cells or tissues using TRIzol (Tiangen Biotech Co., China), and reverse-transcribed with HyperScript III RT SuperMix for qPCR with gDNA Remover (EnzyArtisan, China). Reverse transcription products of different samples were amplified by StepOne Real-Time PCR system (Applied Biosystems, USA) using 2 × S6 Universal SYBR qPCR mix (EnzyArtisan, Shanghai, China) according to the manufacturer's instruction. Data were normalized by the internal control GAPDH (for Human genes examination) or Actin (for Murine genes examination) expression and $2^{-\Delta\Delta Ct}$ method was used to calculate relative expression changes. Sequences of the primers used for qRT-PCR are shown in Supplementary Table S2.

ELISA

Secreted cytokines in cell culture supernatants, sera, BAL or lung homogenates from virus-infected mice were analyzed using mouse IFN-β, IFN-α, IL-6 and CCL2 ELISA kits (Thermo Fisher Scientific, USA) according to the manufacture's instruction.

Flow cytometry analysis

After infected with VSV-GFP or PR8-GFP at the indicated time, cells were collected and re-suspended in PBS. Flow cytometry data were acquired on CytoFLEX S (Beckman Coulter, USA).

Single-cell RNA sequencing data analysis

Publicly available scRNA-seq data of BAL containing 51 samples were acquired from the Gene Expression Omnibus (GEO) database (GSE128033, GSE145926, GSE151928, GSE155249, GSE183974, and GSE197440), which encompassed 21 severely ill patients with COVID-19, 3 mildly ill patients with COVID-19 and 27 healthy controls. Publicly available scRNA-seq data of blood containing 83 samples were also acquired from the GEO database (GSE174072, GSE192391, GSE166992, GSE178404, and GSE149689) which encompassed 45 severely ill patients with COVID-19, 16 severely ill patients with influenza, and 22 healthy controls.

All databases were split according to the samples and filtered with the parameter of 'subset = nCount_RNA >200' by the function of 'subset' provided by Seurat (v4). Then the 'chord' function provided by 'chord' package was utilized to eliminate cells identified as potential doublets from the analysis. The function of 'PercentageFeatureSet' was used to calculate the percentage of all the counts belonging to mitochondrial genes for each cell and only cells that satisfy the criteria of having more than 500 RNA features, over 1000 RNA counts, and a mitochondrial content of less than 30% were retained for further analysis. All filtered data were normalized and scaled by using 'NormalizeDate' and 'ScaleData' function provided by Seurat (v5) toolkit with default parameters. Principal component analysis (PCA) was performed on the integrated expression profile with 50 principal components by using the 'RunPCA()' function with dafault parameters. To compare the differences across different groups of patients, the gene expression profiles of all samples were integrated by using the 'Harmony' function provided by Seurat (v5) and 'RunBBKNN' function providerd by "bbknnR" with default parameters. After integration, data were performed the function of 'FindNeighbors' with the parameters of 'dims = 1:40' which meant that the number of PCs was set to use the top 40 PCs in 50 PCs with more than 80% of explained variance. Then we used the 'RunTSNE' and 'RunUMAP' function to display and separate different cell clusters with the parameter of 'dims = 1:40'.

Cell type of each cluster was annotated if it expresses known lineage markers. Lineage markers in blood samples included the following: cDCs, expression of ('CLEC9A', 'LAMP3', 'CLEC10A'), megakaryocytes ('CMTM5', 'PF4'), monocytes ('CD14', 'CD68'), neutrophils ('CXCR2', 'FCGR3B'). Lineage markers in balf samples included the following: cDCs, expression of ('CLEC9A', 'LAMP3', 'CLEC10A'), Mo-macrophages ('CD14'), alveolar macrophages ('FABP4'), B cells ('CD79A'), T cells ('CD3D'), secretory cells ('MUC5B'), and ciliated cells ('FOXJ1').

After cell annotation, individual cells from each sample were aggregated to form a composite pseudocell, designed to encapsulate the characteristic gene expression patterns of the specific cell type within the sample. The analytical process entailed two primary steps: Initially, cells were grouped based on their similarity, and the gene expression profiles were organized alphabetically by the gene names present across all selected cells. Subsequently, the aggregate gene expression values were determined, normalized by dividing the total gene expression counts and multiplying the result by one million. For detecting and filtering the batch effect among different databases, the pseudocells we obtained in the previous step were performed the function of 'NormalizeData', 'FindVariableFeatures',

'ScaleData', 'RunPCA', 'FindNeighbors', 'FindClusters' provided by Seurat(v5) with dafault parameters, and 'RunUMAP'. The outcome of UMAP analysis was used to judge the batch effect in different projects. If the sample's distribution was effected by the batch effect, we will use the function of "removeBatchEffect" provided by "limma" to remove the batch effect.

The differentially expressed genes between HC group and COVID-19 group in each pesudocell were identified by 'DESeq2' and the GO enrichment analysis of these genes. The 'UpSetR' package facilitated the visualization of gene overlap across all cell types, providing a comprehensive view of shared genetic elements.

Correlation and function enrichment analysis
The spearman correlation analysis was used to identify the correlation between the gene expression value of TOMM34 and other genes, and TOMM34-related genes were filtered by $P < 0.05$ and correlation value > 0.6. The TOMM34-related genes from BAL samples were screened and the GO enrichment analysis of these genes in each subtype was analyzed through 'enrichGO' function provided by 'clusterprofiler' package. The correlation between gene expression count of TOMM34 and indicated genes was analyzed by the 'corrplot' package.

Virus biological safety levels
All experiments with SeV, VSV, IAV, RSV, and SARS-CoV-2 trVLP were conducted in class 2 microbiology safety cabinets in BSL-2 laboratories. All experiments with SARS-CoV-2 were conducted in a class 1 microbiology safety cabinet in a BSL-3 laboratory of Guangzhou Customs District Technology Center.

Ethics
All the mouse experiments were approved (20230703023) and performed according to a protocol approved by the Animal Care and Use Committee (IACUC) of the Institute of Zhejiang University of Technology.

Statistics
For analyzing the gene expression using published scRNA-seq data, the Wilcoxon rank-sum test was used. In details, cells from different samples were integrated according to the same cell types. The pseudo bulk data was constructed by summing up the gene expression levels and taking the average value to summarize the gene expression differences for each state. When comparing the mean gene expression level of each state, samples with fewer than 10 cells in that particular subgroup were excluded from the analysis for removing the bias caused by single cell sequencing methods and cell annotation. The Wilcoxon rank-sum test was used to analyze whether the differences between non-normally

distributed variables or normally distributed variables, judged by the function of "shapiro.test" in R which can perform normality assumption, are statistically significant and the var.test function in R is indeed utilized for testing the homogeneity of variances among groups.

For analyzing the TOMM34 protein expression, publicly available proteomic data of autopsy samples from seven organs were obtained from the COVID-19 Proteome Database (COVIDpro). The Wilcoxon rank-sum test was used to infer the statistical significance of differences for each pair of groups.

For Survival analysis, Overall survival of mices which TOMM34 was knocked out was compared with those without treatment by using the Kaplan–Meier survival curve analysis after performing the proportional hazards(PH) analysis by 'cox.zph' with default parameters. Statistical significance was assessed by log-rank test. Cox proportional hazards regression was used to calculate hazard rate with 95% confidence intervals by using 'coxph' with default parameters.

For qRT-PCR analysis, statistical significance between two groups was determined by unpaired two-tailed Student's t test using GraphPad Prism 8.

Role of funders
The funders played no roles in the study design, data collection, data analysis, interpretation, or the writing of the manuscript.

Results
Viral induction of TOMM34 is positively correlated with the hyperinflammatory state in severely ill patients with COVID-19 and influenza
In order to study the physiological roles of TOMM proteins in antiviral innate immunity, we firstly examined if there were differential expressions of TOMM genes in epithelium and innate immune cells from individuals with and without viral infectious diseases. To this end, we analyzed the transcriptome profiles of BAL cells from healthy individuals (HC, $n = 26$) and patients with severe COVID-19 (COVID-19, $n = 21$) using published single-cell RNA sequencing (scRNA-seq) data.[47–52] Samples of BAL cells from individuals with mild COVID-19 were not selected owing to insufficient numbers. UMAP analysis identified seven major cell types: alveolar macrophages, monocyte-derived macrophages (Mo-macrophages), classical dendritic cells (cDCs), secretory cells, ciliated cells, T cells and B cells (Fig. 1a). It was indicated that the distribution of samples from different datasets were clustered well by the diseases state (Supplementary Fig. S1a). To study the cellular innate immune response to SARS-CoV-2, we conducted differential gene expression analysis in innate immune cells (alveolar macrophages, Mo-macrophages, cDCs) and epithelial cells (secretory cells and ciliated cells) between HC group and COVID-19
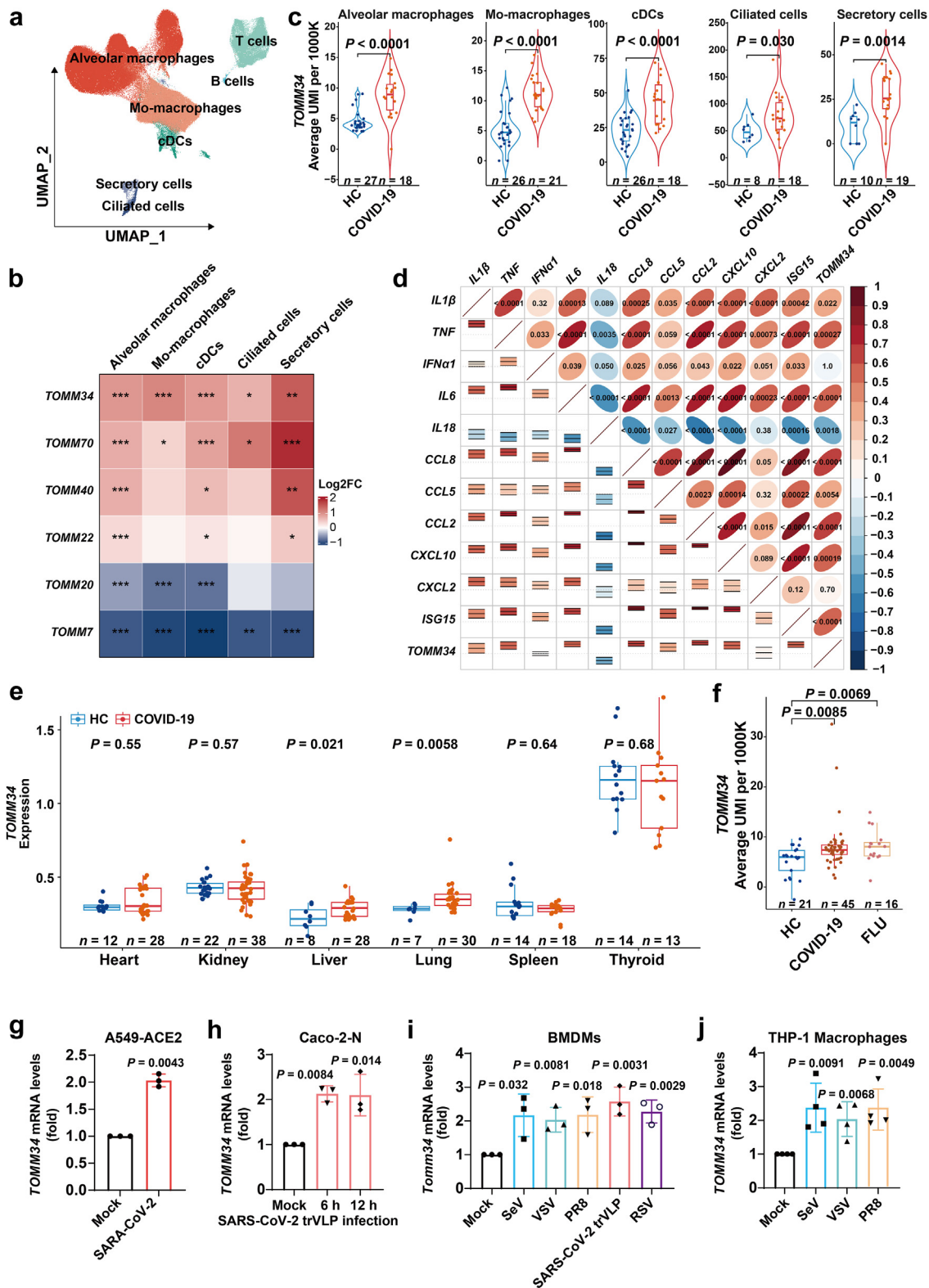
Fig. 1: *TOMM34* mRNA levels are elevated in severely ill patients with COVID-19 and influenza by viral stimulation. **a)** UMAP projection of BAL cell types from healthy controls (HC, *n* = 26) and severe ill patients with COIVD-19 (COVID-19, *n* = 21) using published scRNA-seq data. **b)**

group. It was discovered that 28,479 genes including several *TOMM* genes were differentially expressed (13,107 up and 15,372 down; $P < 0.05$, by DESeq2), and 258 genes were upregulated in all these five cell types of COVID-19 group (Supplementary Fig. S1b). To provide a more comprehensive view of the cellular responses, we displayed the biological processes and pathways that were enriched of those upregulated genes (Supplementary Fig. S1c). *TOMM70,* a well-defined positive regulator of antiviral innate immunity, was found to be transcriptionally upregulated in analyzed cells from COVID-19 group (Fig. 1b and Supplementary Table S3). Compared with other *TOMM* genes, *TOMM34* exhibited the most significant induction (≥1.5-fold, COVID-19 group *versus* HC group) in all analyzed cell clusters, thus attracting our interest. Further gene expression analysis confirmed the increase of *TOMM34* mRNA levels in innate immune cells and epithelial cells from patients with COVID-19 (Fig. 1c and Supplementary Table S3). On the other hand, we uncovered that the genes expressionally correlated with *TOMM34* were enriched in multiple antivirus defense pathways such as the type I IFN production and canonical NF-κB signalling (Supplementary Fig. S1d). These results inspired us to speculate that TOMM34 might be involved in antiviral innate immunity.

Patients with severe COVID-19 commonly exhibit a hyperinflammatory state that is featured by the excessive induction of pro-inflammatory cytokines and chemokines. Our study also manifested that *IL1B, IL6, TNF* and *ISG15* were markedly induced in alveolar macrophages and Mo-macrophages from individuals with severe COVID-19 (Supplementary Fig. S1e and Supplementary Table S3). Moreover, we discovered that *TOMM34* was expressionally correlated with a panel of genes encoding the antiviral effectors and inflammatory

agents in analyzed Mo-macrophages, in which *CCL2,* *CCL8* and *IL6* ranked the top three (Fig. 1d; Supplementary Tables S3 and S4). In addition to the transcription level, we analyzed the differential protein level of TOMM34 in multiple organs from COVID-19 autopsy samples and non-COVID-19 control samples using published proteomic data.[53] The TOMM34 protein was present at statistically higher levels in the lung and the liver from COVID-19 autopsy samples than those from control samples (Fig. 1e and Supplementary Table S3). These findings together implied a tight connection between TOMM34 and pulmonary hyper-inflammation. To extended our observations, we analyzed the differential expression of *TOMM34* in circulating myeloid cells from healthy controls (n = 22) and severely ill patients with COVID-19 (n = 45) or influenza (FLU; n = 16) using published PBMCs scRNA-seq data.[54–60] Four major myeloid cell types: megakaryocytes, monocytes, cDCs, and neutrophils were identified by the UMAP analysis (Supplementary Fig. S2a). Compared to HC group, the mRNA levels of *TOMM34* in circulating monocytes from both COVID-19 group and FLU group were significantly elevated (Fig. 1f and Supplementary Fig. S2b; Supplementary Table S3). Meanwhile, *TOMM34* had a strong expressional correlation with the inflammatory genes such as *IL6* and *CXCL2* in analyzed monocytes when comparing FLU group and HC group (Supplementary Fig. S2c; Supplementary Tables S3 and S4). These data further supported our notion that TOMM34 plays a role in antiviral innate immunity.

To explain the phenomenon that the transcription of *TOMM34* is upregulated in patients with viral infectious diseases, we tested if cellular *TOMM34* mRNA levels would be increased following virus stimulation. As expected, infection of A549-ACE2 cells with SARS-CoV-2

Heatmap illustrating the fold changes (COVID-19 group *vs* HC group) of *TOMM* genes expression in the indicated cell types. The sample size and related power analysis are indicated in Supplementary Table S3. **c)** Violin plot showing the mRNA levels of *TOMM34* in the indicated cell types from HC group and COVID-19 group. The sample size and related power analysis are indicated in Supplementary Table S3. **d)** Gene expression correlation analysis of *TOMM34* and the indicated genes encoding antiviral effectors and inflammatory agents in Mo-macrophages from HC group and COVID-19 group. The shape of the 'ovals' or ellipses is designed to represent the correlation. The upper right triangle displays the *P* values, and the lower left triangle represents the confidence intervals. A central horizontal dashed line within the left lower triangle represents the value of zero. The 95% confidence intervals (CI) for significance are marked by the upper and lower boundaries of the box plot, as shown in Supplementary Table S4. The sample size and related power analysis are indicated in Supplementary Table S3. **e)** Boxplots representing the TOMM34 protein levels in multiple organs from COVID-19 autopsy samples and non-COVID-19 control samples. The sample size and related power analysis are indicated in Supplementary Table S3. **f)** Boxplots showing the mRNA levels of *TOMM34* in the indicated cell types of PBMCs from healthy controls and severely ill patients with COVID-19 or influenza. The UMAP projection of PBMCs myeloid cells are shown in Supplementary Fig. S2a. The sample size and related power analysis are indicated in Supplementary Table S3. **g)** A549-ACE2 (A549 stably expressing ACE2) cells were mock-infected (Mock) or infected with SARS-CoV-2 (multiplicity of infection, MOI = 0.4) for 24 h. qRT-PCR analysis was conducted to examine the relative *TOMM34* mRNA levels. **h)** Caco-2-N cells (Caco-2 stably expressing SARS-CoV-2 nucleocapsid protein) were mock-infected or infected with SARS-CoV-2 trVLP (MOI = 0.1) for the indicated hours. qRT-PCR analysis was conducted to examine the relative *TOMM34* mRNA levels. **i)** Primary murine BMDMs were mock-infected or infected with SeV (20 HA units/ml) and VSV (MOI = 0.1) for 12 h, or with PR8 (MOI = 1), SARS-CoV-2 trVLP (MOI = 0.1) and RSV (MOI = 1) for 24 h. qRT-PCR analysis was conducted to examine the relative *Tomm34* mRNA levels. **j)** THP-1-derived macrophages were mock-infected or infected with SeV (20 HA units/ml) and VSV (MOI = 0.1) for 12 h, or with PR8 (MOI = 1) for 24 h. qRT-PCR analysis was conducted to examine the relative *TOMM34* mRNA levels. Data are represented as mean ± SD calculated from at least three independent experiments (g–j). Wilcoxon rank-sum test (b, c, e, f), two-tailed Student's t test (g–j).

doubled the relative mRNA levels of *TOMM34* in comparison with those in mock-infected (Mock) cells (Fig. 1g). We then used another SARS-CoV-2 infection model, SARS-CoV-2 trVLP-infected Caco-2-N which can be conducted in a Biological Safety Level 2 (BSL-2) laboratory,[43] and indeed observed a similar result (Fig. 1h). Furthermore, myeloid cells such as primary murine BMDMs and human THP-1-derived macrophages were stimulated with diverse viruses to determine the expression of *TOMM34*. In response to pathogenic respiratory RNA viruses [SARS-CoV-2 trVLP, the IAV strain A/Puerto Rico/8/1934 (H1N1; PR8), the RSV strain A-0594] and experimental model RNA viruses (Sendai virus, SeV; vesicular stomatitis virus, VSV), the *Tomm34/TOMM34* mRNA levels in BMDMs and THP-1-derived macrophages were relatively increased (Fig. 1i and j). In contrast, the treatment of THP-1 macrophages with IFN-β, LPS or IL-4 cannot induce TOMM34 expression (Supplementary Fig. S2d). Altogether, our data unveil a positive correlation between the viral induction of TOMM34 and the excessive production of inflammatory agents in severely ill patients with COVID-19 and influenza.

TOMM34 facilitates virus-induced cytokines expression

To examine whether TOMM34 is directly involved in the innate immunity against RNA viruses, we determined the effects of TOMM34 overexpression on the virally induced activation of IFN-β promoter. It has been well-defined that the RIG-I/MDA5 signalling governs the innate immune responses to highly pathogenic RNA viruses such as SARS-CoV-2, IAV and RSV, as well as the experimental model RNA viruses VSV and SeV. Since HEK293T cells are specifically equipped with RIG-I/MDA5 but defect in the TLRs and cGAS-STING pathways, we thus used HEK293T as a cell model here for RNA viruses infection. Following the infection of HEK293T with VSV, the IFN-β promoter-Luciferase (IFN-β-Luc) activities were significantly enhanced upon ectopic expression of TOMM34 or the IFN-β positive regulator TOMM70 (Fig. 2a and Supplementary Fig. S3a). Under the same conditions, however, over-expression of other TOMM proteins such as TOMM6, TOMM20 and TOMM40 had no obvious effects (Fig. 2a and Supplementary Fig. S3a). We further confirmed the positive effects of TOMM34 on the IFN-β-Luc activities induced by a variety of stimuli such as SeV, PR8, RSV, and the duplexed RNA mimic poly(I:C) (Fig. 2b). Moreover, the virally-induced transcriptions of the IFN-β-encoding gene *IFNB1* and the NF-κB-activated genes (*IL6*, *CCL2* and *TNF*) were enhanced upon TOMM34 overexpression (Fig. 2c and Supplementary Fig. S3b). In contrast, the transcription of *ISG54* which reflects the IRF3 activity was not affected (Supplementary Fig. S3b).

Next, we generated a HEK293T cell line defective in *TOMM34* by the CRISPR/Cas9-mediated gene editing

(Supplementary Fig. S3c). In *TOMM34*^{−/−} HEK293T cells, the viral induction of *IFNB1, IL6, CCL2* and *TNF* was markedly decreased in comparison with that in wild-type (WT) HEK293T cells (Fig. 2d and Supplementary Fig. S3d). No difference was observed in the transcription of *ISG54* between WT and *TOMM34*^{−/−} HEK293T cells under the same stimulation. TOMM34 has been previously defined as a cytosolic cochaperone of the Hsp90/Hsp70 complex transferring mitochondrial precursors.[61] The phosphorylation of TOMM34 S93/169 residues are crucial for binding to adaptor 14-3-3 and leaving Hsp70 to process the substrate.[62] During the course of viral infection, however, recovery of TOMM34 WT or the S93/169A mutant in *TOMM34*^{−/−} HEK293T cells substantially rescued the loss of *IFNB1* and *CCL2* mRNA levels (Fig. 2e and Supplementary Fig. S3e), suggesting that the previously undefined role of TOMM34 in antiviral cytokines expression is independent of its function as the Hsp90/Hsp70 cochaperone. Deficiency of TOMM34 sharply promoted viral proliferation, as reflected by the enhanced GFP fluorescence in *TOMM34*^{−/−} HEK293T cells infected with PR8-GFP virus (Fig. 2f). To confirm these results in the respiratory epithelium, we employed WT and *TOMM34*-defective A549 cells to be infected with a variety of RNA viruses. Compared to WT cells, *TOMM34*^{−/−} A549 cells could barely express diverse antiviral cytokines under stimulation with SeV, VSV, PR8 or RSV (Fig. 2g, Supplementary Fig. S3f and g). In addition, we observed a similar phenomenon when using a SARS-CoV-2-infected cell model, as the overexpression of TOMM34 increased the relative transcription levels of *IFNB1* and *TNF* induced by SARS-CoV-2 trVLP (Supplementary Fig. S3h).

We further elucidated the function of murine-derived Tomm34. Mouse embryonic fibroblast (MEF) cell line NIH/3T3, an ideal cell model for studying antiviral innate immunity, was used here to conduct the gain-of-function and loss-of-function assays for *Tomm34*. Consistent with the results observed in HEK293T cells, overexpression of murine Tomm34 substantially increased the mRNA levels of *Ifnb1, Il6, Tnf* and *Ccl2* but not *Isg54* in NIH/3T3 cells stimulated with poly(I:C) (Fig. 2h); whereas the defect in *Tomm34* of NIH/3T3 cells compromised the viral induction of these antiviral cytokines except *Isg54* (Fig. 2i, Supplementary Fig. S3i and j). Meanwhile, *Tomm34*^{−/−} NIH/3T3 cells reconstituting murine Tomm34 restored its capability of producing IFN-β and IL-6 (Fig. 2j and Supplementary Fig. S3k). It was also observed that the Tomm34 deficiency led to an amplified replication of GFP-conjugated VSV in NIH/3T3 cells, as determined by fluorescent microscopy imaging and flow cytometry analysis (Supplementary Fig. S3l and m). Summarily, these results characterise a previously undefined role of TOMM34 in the antiviral cytokines induction.
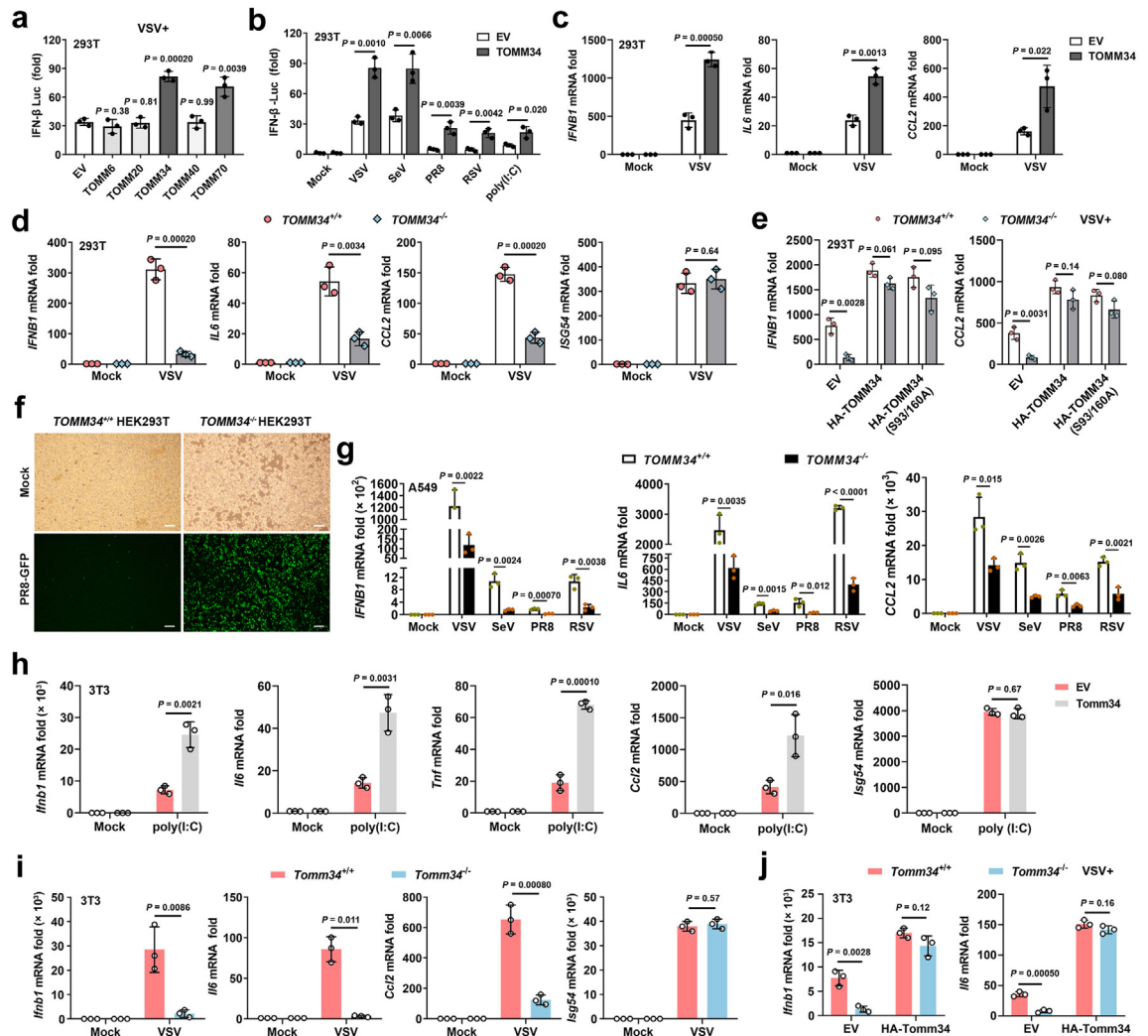
Fig. 2: TOMM34 potentiates antiviral cytokines expression upon virus infection. **a)** Effects of TOMM proteins overexpression on VSV-induced IFN-β promoter activation. HEK293T cells were co-transfected with IFN-β luciferase reporter plasmid (IFN-Beta_pGL3), renilla luciferase plasmid (pRL-TK) plus vectors encoding hemagglutinin (HA)-tagged TOMM proteins as indicated or empty vector (EV) for 24 h, and were then stimulated with VSV (MOI = 0.1) for 12 h. Cell lysates were obtained and subjected to dual luciferase assay. Activities of firefly luciferase were normalized to those of renilla luciferase and shown as fold induction. Protein expression levels are shown in Supplementary Fig. S3a. **b)** Effects of TOMM34 overexpression on IFN-β promoter activation induced by diverse stimuli. Similar to (a), HEK293T cells were transfected with IFN-Beta_pGL3, pRL-TK plus plasmid encoding HA-TOMM34 or EV for 24 h, and were then mock-infected (Mock) or stimulated with VSV, SeV, PR8 (20 HA units/mL), PR8 (MOI = 1), RSV (MOI = 1) and poly(I:C) for 12 h. Cell lysates were obtained and subjected to dual luciferase assay. **c)** Effects of TOMM34 overexpression on antiviral cytokines induction. qRT-PCR analysis of *IFNB1*, *IL6*, and *CCL2* mRNA levels in HEK293T cells transfected with HA-TOMM34 or EV for 24 h, followed by VSV infection for 12 h. The mRNA levels of *TNF* and *ISG54* are shown in Supplementary Fig. S3b. **d)** Impacts on antiviral cytokines induction in the absence of TOMM34. qRT-PCR analysis of *IFNB1*, *IL6*, *CCL2* and *ISG54* mRNA levels in *TOMM34*^{+/+} and *TOMM34*^{−/−} HEK293T cells mock-infected or infected with VSV for 12 h. Protein levels of TOMM34 in *TOMM34*^{+/+} and *TOMM34*^{−/−} HEK293T cells, Supplementary Fig. S3c; mRNA levels of *TNF* in *TOMM34*^{+/+} and *TOMM34*^{−/−} HEK293T cells, Supplementary Fig. S3d. **e)** Effects of TOMM34 recovery on antiviral cytokines induction in *TOMM34*^{−/−} HEK293T cells. qRT-PCR analysis of *IFNB1* and *CCL2* mRNA levels in *TOMM34*^{+/+} and *TOMM34*^{−/−} HEK293T cells that were transfected with EV or vectors encoding HA-tagged TOMM34 and its mutant S93/160A for 24 h, followed by 12 h-VSV infection. Protein expression levels are shown in Supplementary Fig. S3e. **f)** Microscopy imaging of *TOMM34*^{+/+} and *TOMM34*^{−/−} HEK293T cells that were mock-infected or infected with GFP-conjugated PR8 virus (PR8-GFP) for 12 h. Scale bars, 200 μm. **g)** Impacts on antiviral cytokines induction in the absence of TOMM34 in A549 cells. qRT-PCR analysis of *IFNB1*, *IL6* and *CCL2* mRNA levels in *TOMM34*^{+/+} and *TOMM34*^{−/−} A549 cells mock-infected or infected with VSV, SeV (20 HA units/mL), PR8 (MOI = 1) and RSV (MOI = 1) for 12 h. Protein levels of TOMM34 in *TOMM34*^{+/+} and *TOMM34*^{−/−} A549 cells, Supplementary Fig. S3f; mRNA levels of *TNF* in *TOMM34*^{+/+} and *TOMM34*^{−/−} A549 cells, Supplementary Fig. S3g. **h)** Effects of murine Tomm34 overexpression on antiviral cytokines induction. qRT-PCR analysis of *Ifnb1*, *Il6*, *Tnf*, *Ccl2* and *Isg54* mRNA levels in mouse embryonic fibroblast NIH/3T3 cells that
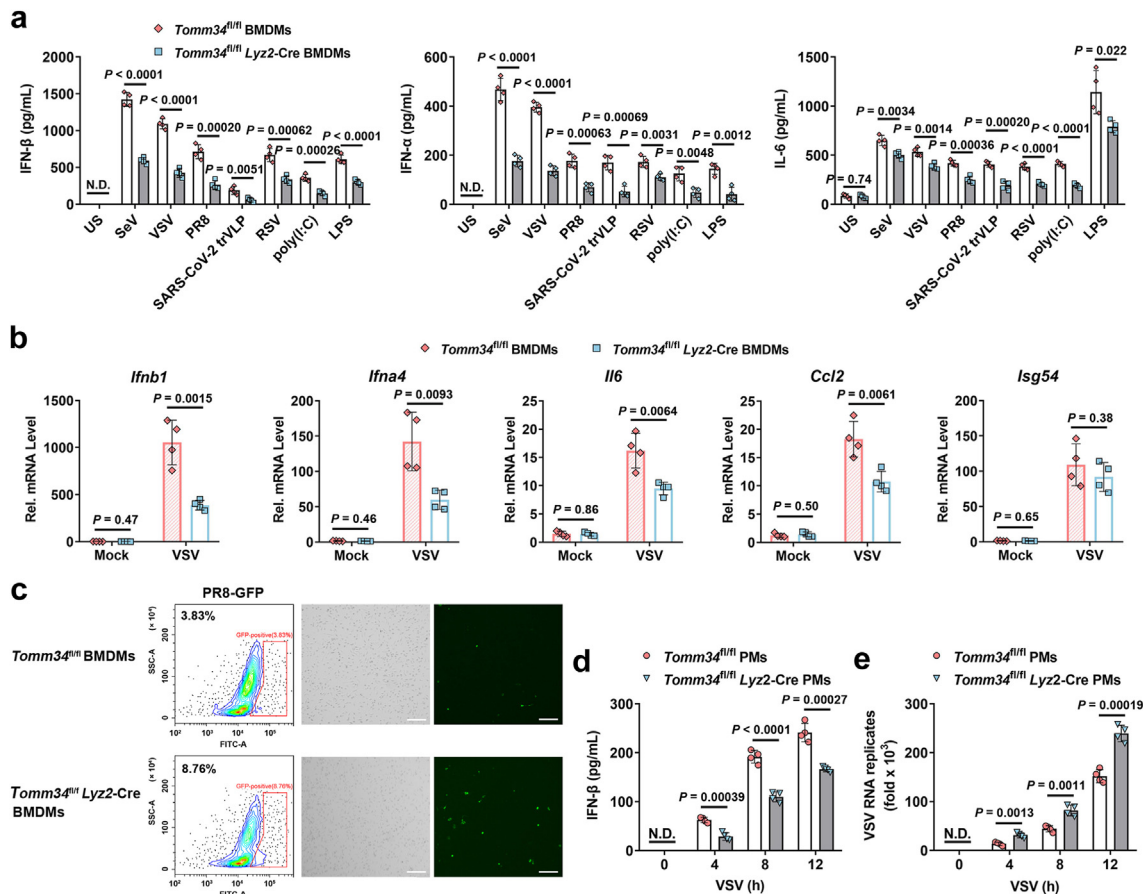
Fig. 3: Tomm34 is pivotal for antiviral innate immunity in primary murine macrophages. **a)** ELISA of IFN-β, IFN-α and IL-6 in supernatants of $Tomm34^{fl/fl}$ and $Tomm34^{fl/fl}$ Lyz2-Cre BMDMs unstimulated (US) or stimulated for 12 h with SeV (20 HA units/mL), VSV (MOI = 0.1), PR8 (MOI = 1), SARS-CoV-2 trVLP (MOI = 0.1), RSV (MOI = 1), poly(I:C) or for 8 h with LPS. Protein levels of Tomm34 in BMDMs collected from $Tomm34^{fl/fl}$ and $Tomm34^{fl/fl}$ Lyz2-Cre mice, Supplementary Fig. S4a; numbers and percentages of BMDMs from $Tomm34^{fl/fl}$ and $Tomm34^{fl/fl}$ Lyz2-Cre mice, Supplementary Fig. S4b and c. **b)** qRT-PCR analysis of Ifnb1, Ifna4, Il6, Ccl2 and Isg54 in $Tomm34^{fl/fl}$ and $Tomm34^{fl/fl}$ Lyz2-Cre BMDMs infected for 8 h with VSV. **c)** Flow cytometry analysis (left graph) and microscopy imaging (right graph) for the replication of PR8-GFP in $Tomm34^{fl/fl}$ and $Tomm34^{fl/fl}$ Lyz2-Cre BMDMs infected with PR8-GFP for 24 h. Scale bars, 200 μm. **d)** ELISA of IFN-β in supernatants of $Tomm34^{fl/fl}$ and $Tomm34^{fl/fl}$ Lyz2-Cre PMs infected for indicated hours with VSV. **e)** qPCR analysis of VSV RNA in PMs that were treated as in (d). Data are represented as mean ± SD calculated from three independent experiments, or are representative of three independent experiments. P values are reported with two significant digits, or shown as "P < 0.0001" (Unpaired two-tailed Student's t test).

Tomm34 deficiency in primary murine macrophages impairs antiviral innate immunity

To demonstrate the physiological role of TOMM34 in antiviral innate immunity, we generated conditional knock-out mice which underwent deletion of loxP-flanked $Tomm34$ alleles ($Tomm34^{fl/fl}$) specifically in myeloid cells via Cre recombinase driven by the myeloid cell-specific lysozyme M promoter ($Lyz2$-Cre), namely

were transfected with plasmid encoding HA-Tomm34 or empty vector for 24 h, and were subsequently mock-stimulated or stimulated with poly(I:C) for 12 h. **i)** Impacts on antiviral cytokines induction in the absence of murine Tomm34. qRT-PCR analysis of Ifnb1, Il6, Ccl2 and Isg54 mRNA levels in $Tomm34^{+/+}$ and $Tomm34^{-/-}$ NIH/3T3 cells that were mock-infected or infected with VSV (MOI = 0.1) for 12 h. Protein levels of Tomm34 in $Tomm34^{+/+}$ and $Tomm34^{-/-}$ NIH/3T3 cells, Supplementary Fig. S3i; mRNA levels of Tnf in $Tomm34^{+/+}$ and $Tomm34^{-/-}$ NIH/3T3 cells cells, Supplementary Fig. S3j. **j)** Effects of Tomm34 recovery on antiviral cytokines induction in $Tomm34^{-/-}$ NIH/3T3 cells. qRT-PCR analysis of Ifnb1 and Il6 mRNA levels in $Tomm34^{+/+}$ and $Tomm34^{-/-}$ NIH/3T3 cells that were transfected with HA-Tomm34 or EV for 24 h, followed by infection with VSV for 12 h. Protein expression levels are shown in Supplementary Figure S2k. Data are represented as mean ± SD calculated from three independent experiments, or are representative of three independent experiments. P values are reported with two significant digits, or shown as "P < 0.0001" (Unpaired two-tailed Student's t test).
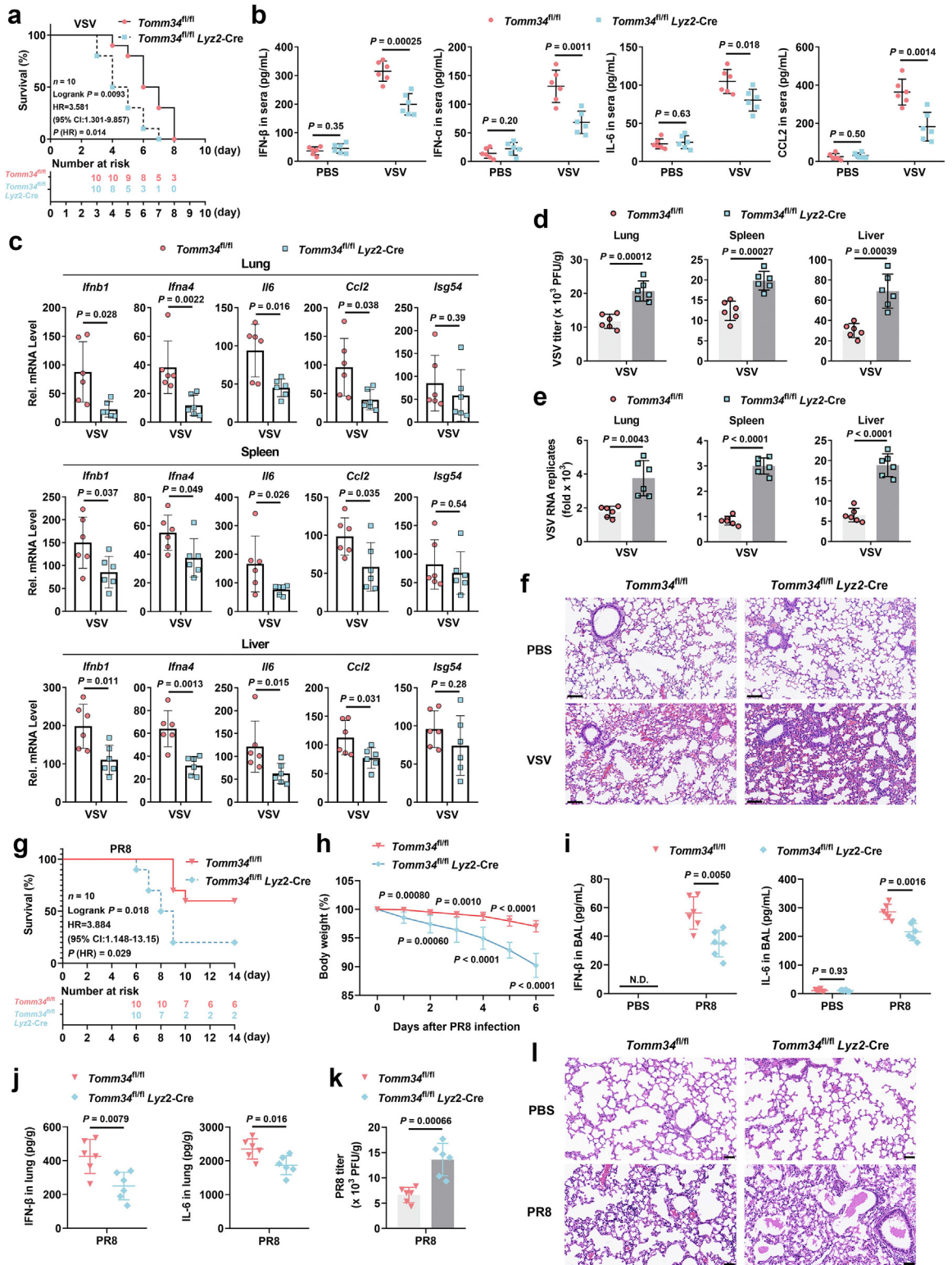
Fig. 4: Tomm34^{fl/fl} Lyz2-Cre mice exhibit increased susceptibility to RNA viruses infection. **a)** Survival (Kaplan–Meier curve) of 7-week-old male *Tomm34*^{fl/fl} and *Tomm34*^{fl/fl} *Lyz2*-Cre mice (*n* = 10) after intraperitoneal injection of VSV (5 × 10^8 PFU per mouse). Time-specific numbers at risk for each group are indicated at the bottom. Mice were infected at day 0 and daily monitored until day 8 (experimnetal end-point as the

Tomm34^{fl/fl} *Lyz2*-Cre (Supplementary Fig. S4a). Compared to *Tomm34*^{fl/fl} mice, *Tomm34*^{fl/fl} *Lyz2*-Cre mice had normal numbers and percentages of BMDMs (Supplementary Fig. S4b and c). We then treated BMDMs obtained from *Tomm34*^{fl/fl} *Lyz2*-Cre mice and their WT littermates with a variety of stimuli. The secretions of IFN-β, IFN-α and IL-6 induced by SeV, VSV, PR8, SARS-CoV-2 trVLP, RSV, poly(I:C) or LPS were significantly lower from *Tomm34*^{fl/fl} *Lyz2*-Cre BMDMs than those from *Tomm34*^{fl/fl} BMDMs (Fig. 3a). *Tomm34*^{fl/fl} *Lyz2*-Cre BMDMs exhibited impaired transcription of *Ifnb1*, *Ifna4*, *Il6* and *Ccl2* after VSV infection, but displayed no statistical difference in the induction of *Isg54* with that of *Tomm34*^{fl/fl} BMDMs (Fig. 3b). In addition, deficiency of Tomm34 in BMDMs promoted the replication of PR8-GFP (Fig. 3c). Consistent with the results observed in BMDMs, the time course of VSV infection showed a constant lower level of secretive IFN-β produced from *Tomm34*^{fl/fl} *Lyz2*-Cre peritoneal macrophages (PMs) than that from *Tomm34*^{fl/fl} PMs (Fig. 3d). Replication of VSV was accordingly potentiated in *Tomm34*^{fl/fl} *Lyz2*-Cre PMs compared with *Tomm34*^{fl/fl} PMs, as determined by qRT-PCR analyses (Fig. 3e). Taken together, our data demonstrate that Tomm34 is indispensable for the antiviral responses of primary murine macrophages.

Myeloid Tomm34 protects mice against viral infection

To further confirm the antiviral significance of Tomm34 *in vivo*, we infected *Tomm34*^{fl/fl} and *Tomm34*^{fl/fl} *Lyz2*-Cre mice with VSV and PR8, respectively. It was illustrated that the mortality of *Tomm34*^{fl/fl} *Lyz2*-Cre mice challenged with VSV was higher than that of the control littermates (Fig. 4a; Supplementary Table S3 and S5). The sera concentrations of IFN-β, IFN-α, IL-6 and CCL2 were significantly decreased in *Tomm34*^{fl/fl} *Lyz2*-Cre mice compared with *Tomm34*^{fl/fl} mice at 24 h after VSV infection (Fig. 4b). Besides, the viral induction of *Ifnb1*,

Ifna4, *Il6* and *Ccl2* rather than *Isg54* were impaired in the lungs, spleens and livers of *Tomm34*^{fl/fl} *Lyz2*-Cre mice (Fig. 4c). Consistently, myeloid deficiency of Tomm34 increased VSV titers and RNA replicates in the lungs, spleens and livers of mice (Fig. 4d and e). H&E staining showed that there was an increased infiltration of inflammatory cells into the lungs of *Tomm34*^{fl/fl} *Lyz2*-Cre mice compared with *Tomm34*^{fl/fl} mice following VSV infection (Fig. 4f).

Upon intranasal infection with a lethal dose of PR8, *Tomm34*^{fl/fl} *Lyz2*-Cre mice showed worse survival and more body weight loss in comparison with those of *Tomm34*^{fl/fl} mice (Fig. 4g and h, Supplementary Fig. S5; Supplementary Tables S3 and S5). The levels of IFN-β and IL-6 in BAL and lung homogenates were higher at Day 3 following PR8 infection in *Tomm34*^{fl/fl} *Lyz2*-Cre mice compared with their control littermates (Fig. 4i and j). Consistently, lung virus titers were lower in *Tomm34*^{fl/fl} *Lyz2*-Cre mice than in *Tomm34*^{fl/fl} mice at Day 3 post-infection with PR8 (Fig. 4k). As a result, we observed more severe injury and enhanced infiltration of immune cells in the lungs of *Tomm34*^{fl/fl} *Lyz2*-Cre mice (Fig. 4l). Collectively, our findings manifest that myeloid Tomm34 is pivotal for establishing the robust innate antiviral state *in vivo*.

TOMM34 promotes NF-κB activation by associating with NEMO

Following RNA virus infection and subsequent formation of the MAVS signalsome at the mitochondria, two downstream signalling pathways TBK1-IRF3 and IKKα/β/γ-NF-κB are activated, leading to the induction of type I IFNs and pathway-specific cytokines.[63] Our data above indicated that TOMM34 potentiated the expression of pro-inflammatory cytokines and chemokines (IL-6, TNF-α, CCL2) driven by NF-κB, but had no impacts on the transcription of IRF3-governed antiviral gene *ISG54*. We thus speculated that TOMM34 functions at the IKKα/β/γ-NF-κB pathway. To validate our speculation,

---

body weight was decreased to 80%). Survival data showing the group, state (0 = survival; 1 = death) and end times of mice were displayed in Supplementary Table S5. The sample size and related power analysis are indicated in Supplementary Table S3. **b)** ELISA of cytokines in serum of mice intraperitoneally injected with VSV (5×10^8 PFU per mouse) or PBS for 24 h ($n = 6$). **c)** qRT-PCR analysis of *Ifnb1*, *Ifna4*, *Il6*, *Ccl2* and *Isg54* mRNA in the lungs, spleens and livers of mice treated as in (b) ($n = 6$). **d)** Plaque assays analyzing VSV titers in the lungs, spleens and livers of mice treated as in (b) ($n = 6$). **e)** qRT-PCR analysis of VSV RNA in the lungs, spleens and livers of mice treated as in (b) ($n = 6$). **f)** Hematoxylin-and-eosin (H&E) staining of sections of lungs from mice treated as in B. Scale bars, 100 μm. **g)** Survival (Kaplan–Meier curve) of 7-week-old male *Tomm34*^{fl/fl} and *Tomm34*^{fl/fl} *Lyz2*-Cre mice after intranasal infection with 50 PFU PR8 ($n = 10$). Time-specific numbers at risk for each group are indicated at the bottom. Mice were infected at day 0 and daily monitored until day 14 (experimnetal end-point as the body weight was decreased to 80%). Survival data showing the group, state (0 = survival; 1 = death) and end times of mice were displayed in Supplementary Table S5. The sample size and related power analysis are indicated in Supplementary Table S3. **h)** Body weights of mice treated as in (g). Mice infected with PR8 were weighted at day 0 (Mock) and daily monitored until any one was dead (day 6, experimnetal end-point). Area under the curve (AUC) for weight change was calculated in Supplementary Fig. S4. **i)** IFN-β and IL-6 levels in BAL from mice at Day 3 after infection with 50 PFU PR8 or PBS ($n = 6$). **j)** IFN-β and IL-6 levels in lung homogenates from mice treated as in (i). **k)** Viral titer in lung homogenates from mice treated as in (i). **l)** H&E staining of sections of lungs from mice treated as in (i). Scale bars, 50 μm. Data are represented as mean ± SD calculated from three independent experiments, or are representative of three independent experiments. *P* values are reported with two significant digits, or shown as "$P < 0.0001$" (Unpaired two-tailed Student's t test).
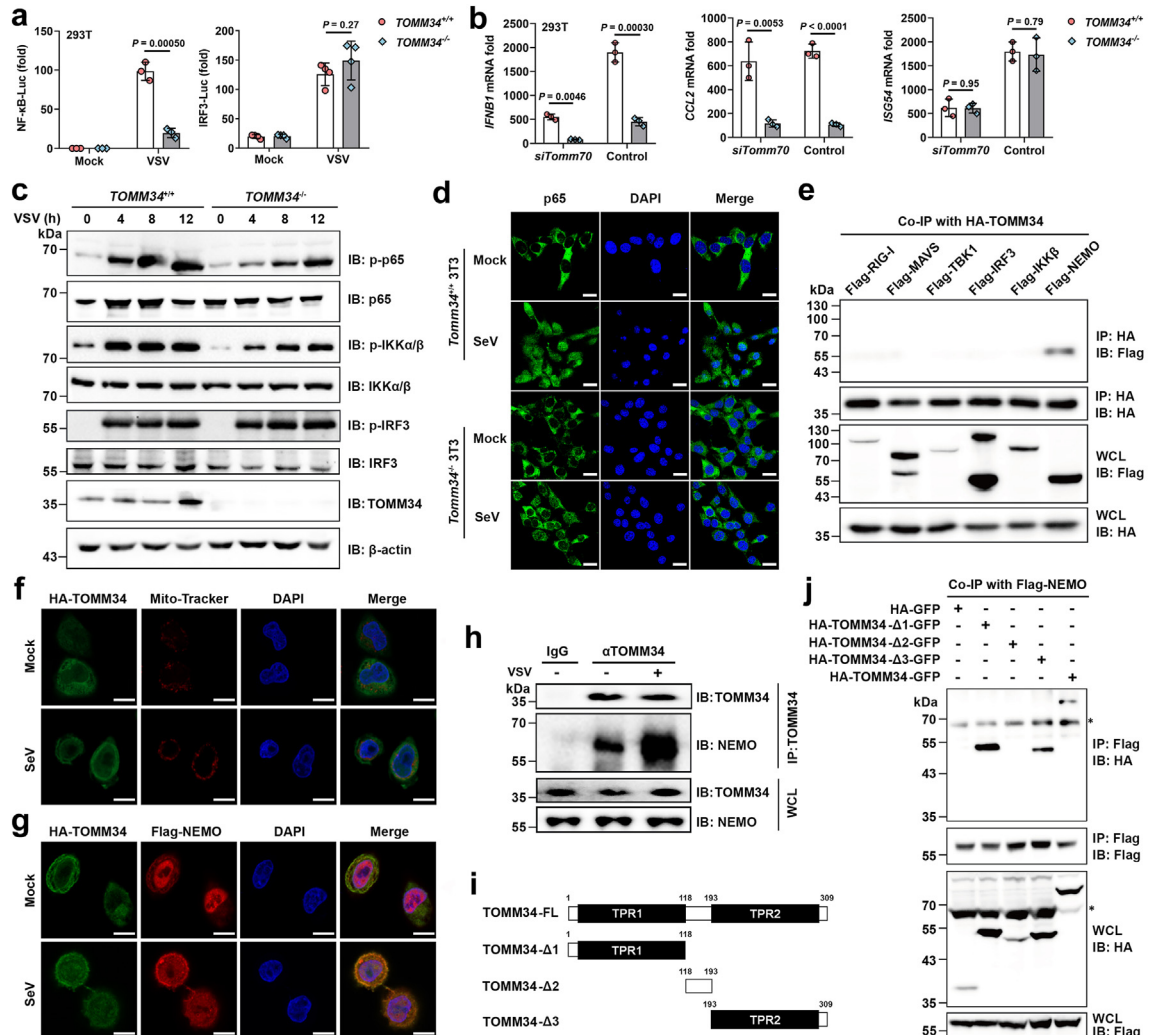
Fig. 5: **TOMM34 interacts with NEMO to facilitate the virally-induced NF-κB activation**. **a)** Impacts on NF-κB and IRF3 promoter activation in the absence of TOMM34. Similar to Fig. 2A, *TOMM34*^{+/+} and *TOMM34*^{−/−} HEK293T cells were transfected with the NF-κB or IRF3 luciferase reporter plasmid plus pRL-TK for 24 h, and were mock-infected or infected with VSV for another 12 h. Cell lysates were obtained and subjected to dual luciferase assay. Activities of firefly luciferase are normalized to those of renilla luciferase and shown as fold induction. **b)** Impacts of *TOMM70*-knocked down on antiviral cytokines induction in *TOMM34*^{−/−} HEK293T cells. qRT-PCR analysis of *IFNB1*, *CCL2* and *ISG54* mRNA levels in *TOMM34*^{+/+} and *TOMM34*^{−/−} HEK293T cells that were treated with TOMM70 siRNA (si*TOMM70*) or scramble siRNA (Control) for 36 h, followed by infection with VSV for 12 h. **c)** Impacts of TOMM34 deficiency on activation of the IKKα/β/γ-NF-κB signalling. Immunoblotting (IB) analysis showing the protein levels of NF-κB p65 and its phosphorylated form (p-p65), IKKα/β and p-IKKα/β, IRF3 and p-IRF3, as well as TOMM34 in *TOMM34*^{+/+} and *TOMM34*^{−/−} HEK293T cells infected with VSV for the indicated time. β-actin was immunoblotted as loading control. **d)** Immunofluorescence staining (with anti-p65 antibody) and miscroscopy imaging of *Tomm34*^{+/+} and *Tomm34*^{−/−} NIH/3T3 cells that were mock-infected or infected with SeV for 12 h. Scale bars, 20 μm. **e)** Co-immunoprecipitation (Co-IP) determining the interaction between TOMM34 and the RIG-I signalling components. HEK293T cells were transfected with HA-Tomm34 and vectors encoding Flag-tagged RIG-I, MAVS, TBK1, IRF3, IKKβ or NEMO for 36 h, and were then subjected to Co-IP using anti-HA beads. Whole cell lysates (WCL) were analyzed by IB with anti-HA and anti-Flag antibodies. **f)** Fluorescent microscopic analysis of TOMM34 localization in HeLa cells transfected with HA-TOMM34. Nucleus and mitochondria were labeled with DAPI and Mito Tracker Red, respectively. Scale bars, 10 μm. The quantification data was shown in Supplementary Fig. S5a. **g)** Fluorescent microscopic analysis of TOMM34 and NEMO colocalization in HeLa cells co-transfected with HA-TOMM34 and Flag-NEMO for 24 h, and were then mock-infeted or infected with SeV for 12 h. Nucleus were labeled with DAPI. Scale bars, 10 μm. The quantification data was shown in Supplementary Fig. S5b. **h)** Immunoprecipitation (IP) examining the endogenous association between TOMM34 and NEMO. HEK293T cells were mock-infected or infected with VSV for 12 h, and were then subjected to IP using IgG or anti-TOMM34 antibodies (αTOMM34). IB analysis was conducted using indicated antibodies. **i)** Scheme for construction of TOMM34 and its deletion mutants. **j)** Co-IP determining the region of TOMM34 protein that is responsible for associating with NEMO. HEK293T cells were co-transfected with plasmid encoding Flag-tagged NEMO (Flag-NEMO) and plasmid encoding N-terminal HA- and C-terminal GFP-tagged

we determined the impacts of TOMM34 deficiency on the activation of NF-κB and IRF3 promoters under viral infection. As expected, TOMM34 absence diminished the activity of NF-κB-Luc rather than that of IRF3-Luc (Fig. 5a). Considering that TOMM70 is also involved in the antiviral type I IFN signalling, we next examined if the functions of TOMM34 and TOMM70 are complementary or redundant to each other. Scramble siRNA and siRNA targeting TOMM70 were transfected into WT and *TOMM34*$^{-/-}$ HEK293T cells, respectively, followed by VSV infection. Knockdown of *TOMM70* decreased the *ISG54* mRNA levels but did not affect *CCL2* mRNA expression upon viral stimulation regardless of the presence of TOMM34 (Fig. 5b). Notably, loss of either TOMM34 or TOMM70 had negative effects on the virus-triggered *IFNB1* transcription, indicating that these two TOMM proteins play distinct roles in the antiviral type I IFN signalling. Further immunoblotting analysis illustrated that the level of activated/phosphorylated NF-κB p65 subunit was relatively lower in *TOMM34*$^{-/-}$ HEK293T cells than that in WT cells during the time course of VSV infection; whereas the virus-induced phosphorylation of IRF3 was unaffected in the absence of TOMM34 (Fig. 5c). Meanwhile, the phosphorylation of IKKα/β which is an upstream event about the NF-κB p65 activation was attenuated in *TOMM34*$^{-/-}$ cells following VSV infection. In line with the diminished phosphorylation of p65, the nuclear translocation of p65 induced by SeV was hindered in *Tomm34*$^{-/-}$ 3T3 cells as determined by immunofluorescence imaging (Fig. 5d).

To understand the detailed mechanism regarding how TOMM34 promotes NF-κB p65 activation, we performed co-immunoprecipitation (Co-IP) assay determining the potential interaction(s) between TOMM34 and key components of the RIG-I-MAVS antiviral signalling pathway. It was obvious that HA-tagged TOMM34 interacted with FLAG-tagged NEMO rather than other components in the RIG-I-mediated antiviral signalling, including RIG-I, MAVS, TBK1, IRF3 or IKKβ (Fig. 5e). Immunofluorescence imaging displayed that HA-TOMM34 was both cytosolically distributed and mitochondrially localized, and showed partial colocalization with Flag-NEMO in resting HeLa cells; while the viral infection triggered the mitochondiral translocation of HA-TOMM34 and significantly promoted its colocalization with Flag-NEMO, as indicated by the quantitative colocalization analysis (Fig. 5f and g, Supplementary Fig. S6a and b). We further conducted immunoprecipitation (IP) assay using anti-TOMM34 antibodies (αTOMM34), and observed an endogenous

association between TOMM34 and NEMO in resting cells (Fig. 5h). It should be notable that viral infection indeed augmented the interaction of TOMM34 with NEMO, as indicated by the increased amounts of endogenous NEMO in the IP products from VSV-infected cells (Fig. 5h, comparing Lanes 2 and 3). Moreover, we generated a series of TOMM34 truncated mutants deleting either one or both two TPR domains (Fig. 5i). As illustrated in Fig. 5j, none of these mutants were able to co-immunoprecipitated with NEMO, indicating that both TPR1 and TPR2 domain of TOMM34 are necessary for its association with NEMO. Truncation of NEMO manifested that either its N-terminal or C-terminal region consisting of ~200 amino acids was indispensable for binding to TOMM34 (Supplementary Fig. S6c and d). We thus conclude that TOMM34 associates with NEMO via its TRP domains and promote the subsequent NF-κB activation.

TOMM34 recruits TRAF6 for NEMO K63-linked polyubiquitination upon virus stimulation

TRAF6 is the ubiquitin E3 ligase responsible for NEMO K63-linked polyubiquitination, a key step in the activation of NEMO and the IKKα/β/γ complex during virus infection.[20] With the aim to dissect how the interaction between TOMM34 and NEMO facilitates the IKKα/β/γ-NF-κB signalling, we examined if there are physiological interactions and interrelationships among TRAF6, TOMM34 and NEMO. For this purpose, we conducted endogenous IP assay using anti-NEMO antibodies (αNEMO) in HEK293T cells mock-infected or infected with SeV. In resting cells, NEMO was only co-immunoprecipitated with TOMM34; while in cells stimulated with SeV, NEMO bound to TRAF6 and had an augmented association with TOMM34 (Fig. 6a). Following immunofluorescence assay showed that the deficiency of Tomm34 in NIH/3T3 cells substantially crippled the interaction between TRAF6 and NEMO (Fig. 6b and Supplementary Fig. S7a).

Next, we determined whether the interaction between TRAF6 and NEMO facilitated by TOMM34 can affect the NEMO K63-linked ubiquitination, which is essential for the IKKα/β/NEMO-NF-κB signalling. HA-tagged ubiquitin (HA-Ub), Flag-NEMO and Myc-TOMM34 were co-expressed in HEK293T cells treated with or without VSV, followed by Co-IP with Flag beads. As shown in Fig. 6c, in both resting cells and VSV-stimulated cells, overexpression of TOMM34 dramatically increased the levels of HA-Ub-conjugated NEMO, and augmented the binding of Flag-NEMO with endogenous TRAF6. Meanwhile, the mutation S94/

TOMM34 (HA-TOMM34-GFP) or its mutants as indicated for 36 h, and were then subjected to Co-IP using anti-Flag beads. IB analysis was conducted using indicated antibodies. Asterisk indicates the nonspecific bands. Data are represented as mean ± SD calculated from three independent experiments, or are representative of three independent experiments. *P* values are reported with two significant digits or shown as "*P* < 0.0001" (Unpaired two-tailed Student's t test).
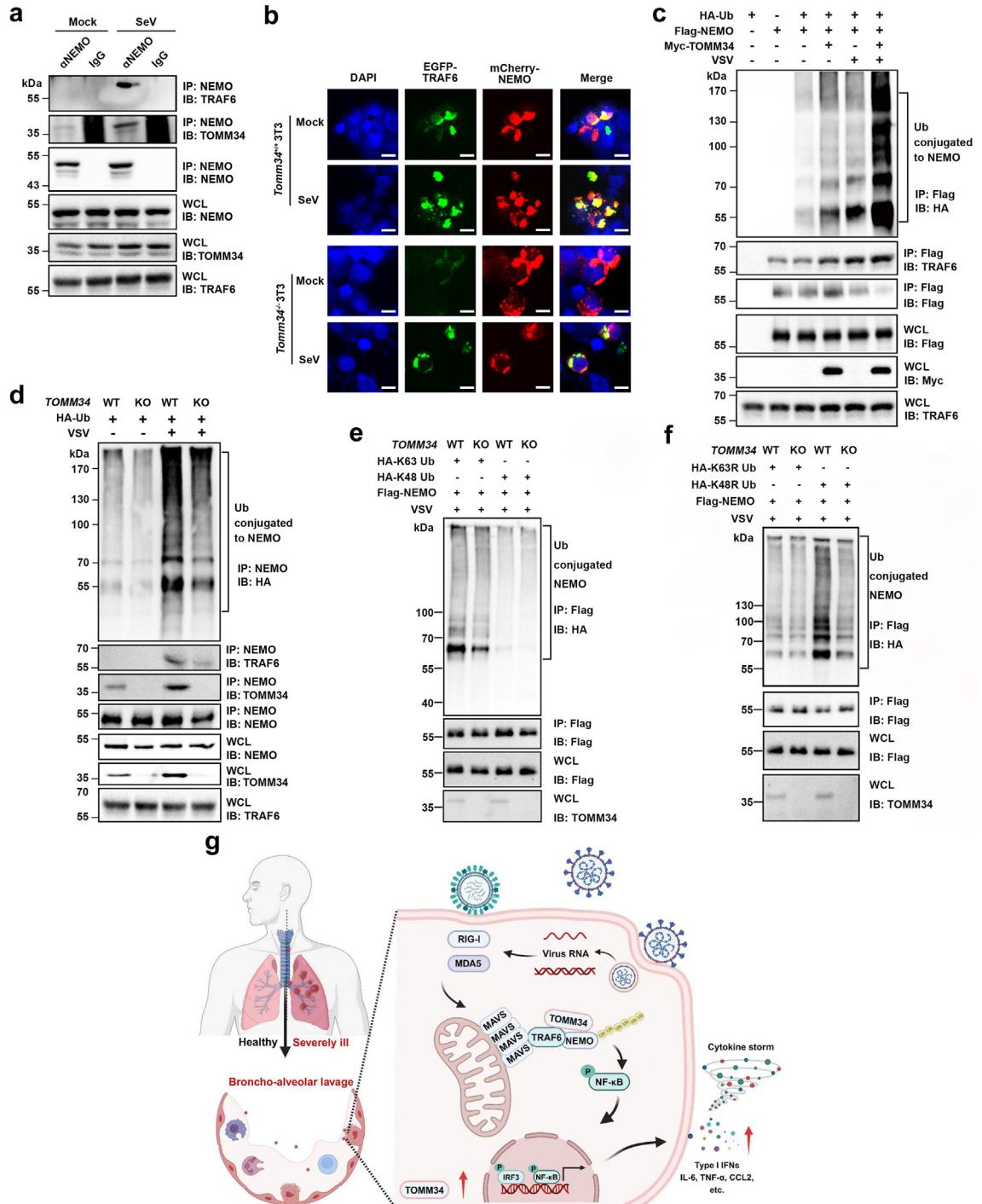
Fig. 6: **TOMM34 promotes the K63-linked polyubiquitination of NEMO under viral stimulation**. a) IP analysis showing the endogenous co-interaction among TOMM34, TRAF6 and NEMO upon viral infection. HEK293T cells were mock-infected or infected with SeV for 12 h, and were then subjected to IP analysis using IgG or anti-NEMO antibodies (αNEMO). IB analysis was conducted using indicated antibodies. b) Fluorescent microscopic analysis of TRAF6 and NEMO colocalization in *Tomm34*$^{+/+}$ and *Tomm34*$^{-/-}$ NIH/3T3 cells co-transfected with plasmids encoding EGFP-tagged TRAF6 and mCherry-tagged NEMO for 24 h, and were then mock-infected or infected with SeV for 12 h. Nucleus was stained with DAPI. Scale bars, 10 μm. c) Effects of TOMM34 overexpression on the ubiquitination of NEMO under viral stimulation. HEK293T cells were transfected with indicated vectors for 24 h, followed by mock-infection or infection with VSV for 12 h. Cells were collected and subjected to IP using anti-Flag beads. IB analysis was conducted using indicated antibodies. d) Impacts of TOMM34 deficiency on the ubiquitination of NEMO

160A of TOMM34 did not impair its augmentation effect on the virally induced ubiquitination of NEMO, further supporting the notion that the indispensable role of TOMM34 in transducing antiviral signal is independent of its function as the Hsp90/Hsp70 cochaperone (Supplementary Fig. S7b). We further conducted endogenous IP using anti-NEMO antibodies in $TOMM34^{-/-}$ HEK293T and WT cells. A decreased level of NEMO ubiquitination was observed in TOMM34-deficient cells compared with WT cells under both quiescent and VSV-stimulated conditions (Fig. 6d). Since NEMO undergoes both K63-linked and K48-linked polyubiquitin conjunction, we sought to figure out which type of NEMO polyubiquitination was affected by TOMM34. Co-IP results showed that both the deficiency and the overexpression of TOMM34 only enhanced the K63-linked polyubiquitination of NEMO, but had no impacts on its K48-linked polyubiquitin conjunction (Fig. 6e and Supplementary Fig. S7c). We observed a consistent result when expressing HA-K63R and HA-K48R polyubiquitin chains in WT and $TOMM34^{-/-}$ HEK293T cells under viral stimulation, as indicated by the compromised non-K48-linked polyubiquitination of NEMO in the absence of TOMM34 (Fig. 6f). Thus, our data suggest that TOMM34 promotes the K63 ubiquitination of NEMO by linking TRAF6 to NEMO upon virus infection.

Discussion

Molecular details underlying the virus-induced formation of MAVS signalsome at the mitochondria has been considerably elucidated, showing that RIG-I/MDA5 activated by viral RNA triggers MAVS to aggregate and form a complex with multiple ubiquitin E3 ligases including TRAF6.[64–66] In spite of that, how the MAVS signalsome recruits downstream signalling components which reside in the cytosol remains largely unknown. Our present work provides evidence that TOMM34 is a component of the MAVS signalsome facilitating the antiviral signal transduction. Deficiency of TOMM34 impaired the expression of type I IFNs, pro-inflammatory cytokines and chemokines, which potentiated the survival of RNA viruses both in cells and *in vivo*. Further investigation manifested that the MAVS-downstream signalling cascade affected by TOMM34 is IKKα/β/NEMO-NF-κB rather than TBK1-IRF3. TOMM34 interacts with NEMO through its TPR domains; when antiviral signalling is activated, it serves as an adaptor linking NEMO to TRAF6, ultimately boosting the antiviral response through the IKKα/β/γ-NF-κB signalling cascade. We thus propose a model for the role of TOMM34 in antiviral innate immunity (Fig. 6g): Infection with SARS-CoV-2, IAV and other RNA viruses induce the expression of TOMM34 in the lung epithelium and innate immune cells. The co-interaction with TOMM34 sets up a bridge between NEMO and TRAF6, which guides NEMO to the MAVS signalsome and promotes the K63-linked ubiquitination of NEMO by TRAF6. As a result, the activation of NF-κB and production of downstream antiviral cytokines are provoked. Crystallization of the TRAF6-TOMM34-NEMO complex is ongoing to provide further molecular details into the MAVS signalsome upon antiviral signal transduction.

Aberrant expression of TOMM34 has been observed in a variety of cancers including colorectal, breast and ovarian tumours, and was thought to be associated with poor prognosis.[34,38,67,68] Here we reported an upregulation of TOMM34 transcription in circulating monocytes, lung epithelium and innate immune cells from severely ill patients with COVID-19 and influenza. The final outcome of our UMAP analysis revealed that the major influencing factor of samples difference is the diseases state rather than other confounding factors. Moreover, our data suggested that the viral induction of TOMM34 might be positively correlated to the hyperinflammatory state in severely ill patients with viral infectious diseases. Our cell models further validated that the TOMM34 transcription was elevated by not only SARS-CoV-2 but also other RNA viruses in both macrophages and epithelial cells. Therefore, the expression of TOMM34 in PBMCs might be applied as a clinical indicator to predict the severity of patients infected with RNA viruses. Still, the mechanism of TOMM34 upregulation upon RNA virus infection remains unclear. Nuclear respiratory factor-1 (NRF-1) is a potential candidate responsible for the activated transcription of TOMM34, as previous ChIP-Seq assay has identified TOMM34 as a target gene of NRF-1.[69] Future promoter assay together with the transcription factor binding site prediction would be conducted to find out the certain transcription factors that upregulate the expression of TOMM34.

under viral stimulation. $TOMM34^{+/+}$ and $TOMM34^{-/-}$ HEK293T cells were transfected with HA-Ub for 24 h, and were mock-infected or infected with VSV for 12 h. Ubiquitination of endogenous NEMO were assessed by IP (using anti-NEMO antibodies and protein A/G beads) and IB (using indicated antibodies) analysis. **e and f)** Effects of TOMM34 deficiency on the K48- and K63-linked ubiquitination of NEMO under viral stimulation. $TOMM34^{+/+}$ and $TOMM34^{-/-}$ HEK293T cells were transfected with plasmids expressing various HA-Ub (K48 only, K63 only, K48R, and K63R as indicated) and Flag-NEMO for 24 h, followed by infection with VSV for 12 h. Cells were subjected to IP (using anti-Flag beads) and IB analysis (using indicated antibodies) for determining the type of NEMO polyubiquitination. Data are representative of three independent experiments. **g)** A model for TOMM34 facilitates antiviral innate immunity. Upon RNA virus infection, cellular TOMM34 is induced to guide NEMO toward TARF6 in the MAVS signalsome, thus facilitating the K63-linked ubiquitination of NEMO, activation of NF-κB signalling and subsequent production of antiviral cytokines.

Classic subunits of TOMM such as TOMM20 and TOMM40, are anchored at the outer membrane of mitochondria and responsible for the import of mitochondrial proteins.[70] As a noncanonical TOMM protein, TOMM34 is distributed in the cytosol and also mitochondrially located. Whether TOMM34 is a redundant member in the TOMM family or has its unique activity is thus intriguing to be investigated. Our study revealed a previously undefined role of TOMM34 as an antiviral signalling modulator. In resting cells, TOMM34 interacts with NEMO in the cytosol; while antiviral signal is transduced, the mitochondrially-translocated tendency of TOMM34 guides NEMO to TRAF6 which is ahead complexed with MAVS aggregates at the mitochondria. The presence of TOMM34 intensively enhances the interaction between NEMO and TARF6, promoting the K63-linked ubiquitination of NEMO and downstream NF-κB activation. Therefore, TOMM34 plays a distinct role in antiviral innate immunity from TOMM70 which functions by linking MAVS to the TBK1-IRF3 cascade. Furthermore, our research disclosed that both TPR1 and TPR2 domains are necessary for TOMM34 to interact with NEMO. In contrast, the interaction of TOMM34 with Hsp70 only requires TRP1 domain, while TRP2 domain binds specifically to Hsp90.[62] Besides the NF-κB signalling, TOMM34 may also exhibit antiviral activity through other cellular pathways or biological processes. According to a previous study, TOMM34 can interact with ATP5B to promote oxidative phosphorylation (OXPHOS) and ATP production.[71] The activity of OXPHOS is indispensable in the RLR-mediated antiviral innate immunity, and glycolysis inhibits the RLR signalling by producing lactate.[72–74] It is thus reasonable to speculate and further validate that TOMM34 can exert its antiviral activity by interfering with cell metabolism.

Since TOMM34 is a critical regulator of antiviral response, manipulating the level of TOMM34 might be a strategy for innate immunity-based therapy. For instance, the activator of TOMM34 expression may enhance antiviral innate immunity to restrain viral replication in the early phase of virus infection, and inhibitors of TOMM34 are potential therapeutic agents for hyperinflammation. On the other hand, TOMM34 is also a potential target that is antagonised by viral proteins, since repressing key molecules in the antiviral signalling is a major strategy for virus to escape from immune surveillance. For instance, SARS-CoV-2 ORF9b associates with TOMM70 to suppress the type I IFN response; while its Nsp5 protein prevents the NF-κB phosphorylation and activation by cleaving TAB1 and NEMO.[41,75] Future study of the TOMM34-interactome upon virus infection is intriguing to discover the viral immune evasion strategies that target TOMM34 and undermine related processes.

Although this work have uncovered the correlation between TOMM34 and inflammatory activation in PBMCs from patients with influenza, lacking the scRNA data of BAL cells limited the exploration of TOMM34's physiological significance in this population. Besides, the mechanism of how TOMM34 is induced upon viral infection was not fully interpreted. Furthermore, our present data is insufficient to conclude that targeting TOMM34 is a feasible clinical intervention for the virally induced hyperinflammation. To approach TOMM34 as a potential therapeutic target in clinical trials, a cohort study integrated with a meticulous evaluation are imperative to be conducted in the future.

Contributors
N. Qi, Q. Shi, W. Zhu, and P. Zhang conceived and designed the study. Q. Shi, P. Zhang, R. Hou, S. Yin, Y. Zou, S. Jiao, B. Zheng, Y. Chen, T. Zhan, Y. Liu and W. Zhu conducted experiments. L. Shi established the cell model of SARS-CoV-2 infection. Q. Shi, P. Zhang, Q. Hu, T. Zhang, F. Chen, W. Zhu and N. Qi analyzed the data. N. Qi, W. Zhu, Y. Liu and Q. Shi prepared the manuscript and revised the manuscript. All authors have read and approved the final version of the manuscript.

Declaration of interests
The authors have declared that no conflicts of interest exist.

Appendix A. Supplementary data
Supplementary data related to this article can be found at https://doi.org/10.1016/j.ebiom.2024.105343.

References
1. Wu J, Shi Y, Pan X, et al. SARS-CoV-2 ORF9b inhibits RIG-I-MAVS antiviral signaling by interrupting K63-linked ubiquitination of NEMO. *Cell Rep.* 2021;34(7):108761.
2. Thorne LG, Reuschl AK, Zuliani-Alvarez L, et al. SARS-CoV-2 sensing by RIG-I and MDA5 links epithelial infection to macrophage inflammation. *EMBO J.* 2021;40(15):e107826.
3. Sasai M, Shingai M, Funami K, et al. NAK-associated protein 1 participates in both the TLR3 and the cytoplasmic pathways in type I IFN induction. *J Immunol.* 2006;177(12):8676–8683.
4. Pichlmair A, Schulz O, Tan CP, et al. RIG-I-mediated antiviral responses to single-stranded RNA bearing 5'-phosphates. *Science.* 2006;314(5801):997–1001.
5. Liu P, Jamaluddin M, Li K, Garofalo RP, Casola A, Brasier AR. Retinoic acid-inducible gene I mediates early antiviral response and Toll-like receptor 3 expression in respiratory syncytial virus-infected airway epithelial cells. *J Virol.* 2007;81(3):1401–1411.
6. Kawai T, Takahashi K, Sato S, et al. IPS-1, an adaptor triggering RIG-I- and Mda5-mediated type I interferon induction. *Nat Immunol.* 2005;6(10):981–988.
7. Meylan E, Curran J, Hofmann K, et al. Cardif is an adaptor protein in the RIG-I antiviral pathway and is targeted by hepatitis C virus. *Nature.* 2005;437(7062):1167–1172.

8   Seth RB, Sun L, Ea CK, Chen ZJ. Identification and characterization of MAVS, a mitochondrial antiviral signaling protein that activates NF-kappaB and IRF 3. *Cell*. 2005;122(5):669–682.

9   Xu LG, Wang YY, Han KJ, Li LY, Zhai Z, Shu HB. VISA is an adapter protein required for virus-triggered IFN-beta signaling. *Mol Cell*. 2005;19(6):727–740.

10 Wathelet MG, Lin CH, Parekh BS, Ronco LV, Howley PM, Maniatis T. Virus infection induces the assembly of coordinately activated transcription factors on the IFN-beta enhancer in vivo. *Mol Cell*. 1998;1(4):507–518.

11 Lin R, Genin P, Mamane Y, Hiscott J. Selective DNA binding and association with the CREB binding protein coactivator contribute to differential activation of alpha/beta interferon genes by interferon regulatory factors 3 and 7. *Mol Cell Biol*. 2000;20(17):6342–6353.

12 Kim T, Kim TY, Lee WG, Yim J, Kim TK. Signaling pathways to the assembly of an interferon-beta enhanceosome. Chemical genetic studies with a small molecule. *J Biol Chem*. 2000;275(22): 16910–16917.

13 da Costa LS, Outlioua A, Anginot A, Akarid K, Arnoult D. RNA viruses promote activation of the NLRP3 inflammasome through cytopathogenic effect-induced potassium efflux. *Cell Death Dis*. 2019;10(5):346.

14 Zheng M, Karki R, Williams EP, et al. TLR2 senses the SARS-CoV-2 envelope protein to produce inflammatory cytokines. *Nat Immunol*. 2021;22(7):829–838.

15 Zhao Y, Kuang M, Li J, et al. SARS-CoV-2 spike protein interacts with and activates TLR41. *Cell Res*. 2021;31(7):818–820.

16 Qudus MS, Tian M, Sirajuddin S, et al. The roles of critical pro-inflammatory cytokines in the drive of cytokine storm during SARS-CoV-2 infection. *J Med Virol*. 2023;95(4):e28751.

17 Sefik E, Qu R, Junqueira C, et al. Inflammasome activation in infected macrophages drives COVID-19 pathology. *Nature*. 2022;606(7914):585–593.

18 Junqueira C, Crespo A, Ranjbar S, et al. FcgammaR-mediated SARS-CoV-2 infection of monocytes activates inflammation. *Nature*. 2022;606(7914):576–584.

19 Cheong JG, Ravishankar A, Sharma S, et al. Epigenetic memory of coronavirus infection in innate immune cells and their progenitors. *Cell*. 2023;186(18):3882–3902.e24.

20 Wang C, Deng L, Hong M, Akkaraju GR, Inoue J, Chen ZJ. TAK1 is a ubiquitin-dependent kinase of MKK and IKK. *Nature*. 2001;412(6844):346–351.

21 Chen ZJ, Parent L, Maniatis T. Site-specific phosphorylation of IkappaBalpha by a novel ubiquitination-dependent protein kinase activity. *Cell*. 1996;84(6):853–862.

22 Yamaoka S, Courtois G, Bessia C, et al. Complementation cloning of NEMO, a component of the IkappaB kinase complex essential for NF-kappaB activation. *Cell*. 1998;93(7):1231–1240.

23 Rothwarf DM, Zandi E, Natoli G, Karin M. IKK-gamma is an essential regulatory subunit of the IkappaB kinase complex. *Nature*. 1998;395(6699):297–300.

24 Mercurio F, Murray BW, Shevchenko A, et al. IkappaB kinase (IKK)-associated protein 1, a common component of the heterogeneous IKK complex. *Mol Cell Biol*. 1999;19(2):1526–1538.

25 Hameedi MA, E TP, Garvin MR, et al. Structural and functional characterization of NEMO cleavage by SARS-CoV-2 3CLpro. *Nat Commun*. 2022;13(1):5285.

26 Wang D, Fang L, Wei D, et al. Hepatitis A virus 3C protease cleaves NEMO to impair induction of beta interferon. *J Virol*. 2014;88(17):10252–10258.

27 Muscolino E, Schmitz R, Loroch S, et al. Herpesviruses induce aggregation and selective autophagy of host signalling proteins NEMO and RIPK1 as an immune-evasion mechanism. *Nat Microbiol*. 2020;5(2):331–342.

28 Zotta A, Hooftman A, O'Neill LAJ. SARS-CoV-2 targets MAVS for immune evasion. *Nat Cell Biol*. 2021;23(7):682–683.

29 Qin Y, Xue B, Liu C, et al. NLRX1 mediates MAVS degradation to attenuate the hepatitis C virus-induced innate immune response through PCBP2. *J Virol*. 2017;91(23):e01264.

30 Huang K, Pei S, Sun Y, et al. Mitofusin 1-mediated redistribution of mitochondrial antiviral signaling protein promotes type 1 interferon response in human cytomegalovirus infection. *Microbiol Spectr*. 2023;11(2):e0461522.

31 Hou J, Han L, Zhao Z, et al. USP18 positively regulates innate antiviral immunity by promoting K63-linked polyubiquitination of MAVS. *Nat Commun*. 2021;12(1):2970.

32 Neupert W, Herrmann JM. Translocation of proteins into mitochondria. *Annu Rev Biochem*. 2007;76:723–749.

33 Baker MJ, Frazier AE, Gulbis JM, Ryan MT. Mitochondrial protein-import machinery: correlating structure with function. *Trends Cell Biol*. 2007;17(9):456–464.

34 Muller P, Coates PJ, Nenutil R, et al. Tomm34 is commonly expressed in epithelial ovarian cancer and associates with tumour type and high FIGO stage. *J Ovarian Res*. 2019;12(1):30.

35 Kreimendahl S, Rassow J. The mitochondrial outer membrane protein Tom70-mediator in protein traffic, membrane contact sites and innate immunity. *Int J Mol Sci*. 2020;21(19):7262.

36 Kato H, Mihara K. Identification of Tom5 and Tom6 in the pre-protein translocase complex of human mitochondrial outer membrane. *Biochem Biophys Res Commun*. 2008;369(3):958–963.

37 Hill K, Model K, Ryan MT, et al. Tom40 forms the hydrophilic channel of the mitochondrial import pore for preproteins [see comment]. *Nature*. 1998;395(6701):516–521.

38 Aleskandarany MA, Negm OH, Rakha EA, et al. TOMM34 expression in early invasive breast cancer: a biomarker associated with poor outcome. *Breast Cancer Res Treat*. 2012;136(2): 419–427.

39 Abe Y, Shodai T, Muto T, et al. Structural basis of presequence recognition by the mitochondrial protein import receptor Tom20. *Cell*. 2000;100(5):551–560.

40 Liu XY, Wei B, Shi HX, Shan YF, Wang C. Tom70 mediates activation of interferon regulatory factor 3 on mitochondria. *Cell Res*. 2010;20(9):994–1011.

41 Jiang HW, Zhang HN, Meng QF, et al. SARS-CoV-2 Orf9b suppresses type I interferon responses by targeting TOM70. *Cell Mol Immunol*. 2020;17(9):998–1000.

42 Gao X, Zhu K, Qin B, Olieric V, Wang M, Cui S. Crystal structure of SARS-CoV-2 Orf9b in complex with human TOM70 suggests unusual virus-host interactions. *Nat Commun*. 2021;12(1):2843.

43 Ju X, Zhu Y, Wang Y, et al. A novel cell culture system modeling the SARS-CoV-2 life cycle. *PLoS Pathog*. 2021;17(3):e1009439.

44 Zhou P, Yang XL, Wang XG, et al. A pneumonia outbreak associated with a new coronavirus of probable bat origin. *Nature*. 2020;579(7798):270–273.

45 Zhao X, Lin X, Li P, et al. Expanding the tolerance of segmented Influenza A Virus genome using a balance compensation strategy. *PLoS Pathog*. 2022;18(8):e1010756.

46 Ran FA, Hsu PD, Wright J, Agarwala V, Scott DA, Zhang F. Genome engineering using the CRISPR-Cas9 system. *Nat Protoc*. 2013;8(11):2281–2308.

47 Grant RA, Morales-Nebreda L, Markov NS, et al. Circuits between infected macrophages and T cells in SARS-CoV-2 pneumonia. *Nature*. 2021;590(7847):635–641.

48 Liao M, Liu Y, Yuan J, et al. Single-cell landscape of bronchoalveolar immune cells in patients with COVID-19. *Nat Med*. 2020;26(6): 842–844.

49 Liegeois M, Bai Q, Fievez L, et al. Airway macrophages encompass transcriptionally and functionally distinct subsets altered by smoking. *Am J Respir Cell Mol Biol*. 2022;67(2):241–252.

50 Morse C, Tabib T, Sembrat J, et al. Proliferating SPP1/MERTK-expressing macrophages in idiopathic pulmonary fibrosis. *Eur Respir J*. 2019;54(2):1802441.

51 Mould KJ, Moore CM, McManus SA, et al. Airspace macrophages and monocytes exist in transcriptionally distinct subsets in healthy adults. *Am J Respir Crit Care Med*. 2021;203(8):946–956.

52 Reyfman PA, Malsin ES, Khuder B, et al. A novel MIP-1-expressing macrophage subtype in BAL fluid from healthy volunteers. *Am J Respir Cell Mol Biol*. 2023;68(2):176–185.

53 Nie X, Qian L, Sun R, et al. Multi-organ proteomic landscape of COVID-19 autopsies. *Cell*. 2021;184(3):775–791.e14.

54 Amrute JM, Perry AM, Anand G, et al. Cell specific peripheral immune responses predict survival in critical COVID-19 patients. *Nat Commun*. 2022;13(1):882.

55 Choi B, Kang CK, Park S, et al. Single-cell transcriptome analyses reveal distinct gene expression signatures of severe COVID-19 in the presence of clonal hematopoiesis. *Exp Mol Med*. 2022;54(10): 1756–1765.

56 Lee JS, Park S, Jeong HW, et al. Immunophenotyping of COVID-19 and influenza highlights the role of type I interferons in development of severe COVID-19. *Sci Immunol*. 2020;5(49):eabd1554.

57 Thompson EA, Cascino K, Ordonez AA, et al. Metabolic programs define dysfunctional immune responses in severe COVID-19 patients. *Cell Rep*. 2021;34(11):108863.

58 Wilk AJ, Lee MJ, Wei B, et al. Multi-omic profiling reveals widespread dysregulation of innate immunity and hematopoiesis in COVID-19. *J Exp Med*. 2021;218(8):e20210582.

59 Youngs J, Provine NM, Lim N, et al. Identification of immune correlates of fatal outcomes in critically ill COVID-19 patients. *PLoS Pathog.* 2021;17(9):e1009804.

60 Zhang Y, Zong L, Zheng Y, et al. A single-cell atlas of the peripheral immune response in patients with influenza A virus infection. *iScience.* 2023;26(12):108507.

61 Faou P, Hoogenraad NJ. Tom34: a cytosolic cochaperone of the Hsp90/Hsp70 protein complex involved in mitochondrial protein import. *Biochim Biophys Acta.* 2012;1823(2):348–357.

62 Trcka F, Durech M, Man P, Hernychova L, Muller P, Vojtesek B. The assembly and intermolecular properties of the Hsp70-Tomm34-Hsp90 molecular chaperone complex. *J Biol Chem.* 2014;289(14):9887–9901.

63 Shi Y, Yuan B, Qi N, et al. An autoinhibitory mechanism modulates MAVS activity in antiviral innate immune response. *Nat Commun.* 2015;6:7811.

64 Wu B, Peisley A, Tetrault D, et al. Molecular imprinting as a signal-activation mechanism of the viral RNA sensor RIG-I. *Mol Cell.* 2014;55(4):511–523.

65 Liu S, Chen J, Cai X, et al. MAVS recruits multiple ubiquitin E3 ligases to activate antiviral signaling cascades. *Elife.* 2013;2:e00785.

66 Hou F, Sun L, Zheng H, Skaug B, Jiang QX, Chen ZJ. MAVS forms functional prion-like aggregates to activate and propagate antiviral innate immune response. *Cell.* 2011;146(3):448–461.

67 Zhang B, Wang J, Wang X, et al. Proteogenomic characterization of human colon and rectal cancer. *Nature.* 2014;513(7518):382–387.

68 Zanphorlin LM, Lima TB, Wong MJ, et al. Heat shock protein 90 kDa (Hsp90) has a second functional interaction site with the mitochondrial import receptor Tom70. *J Biol Chem.* 2016;291(36):18620–18631.

69 Satoh J, Kawana N, Yamamoto Y. Pathway analysis of ChIP-seq-based NRF1 target genes suggests a logical hypothesis of their involvement in the pathogenesis of neurodegenerative diseases. *Gene Regul Syst Bio.* 2013;7:139–152.

70 Becker T, Pfannschmidt S, Guiard B, et al. Biogenesis of the mitochondrial TOM complex: Mim1 promotes insertion and assembly of signal-anchored receptors. *J Biol Chem.* 2008;283(1):120–127.

71 Jin P, Jiang J, Zhou L, et al. Disrupting metformin adaptation of liver cancer cells by targeting the TOMM34/ATP5B axis. *EMBO Mol Med.* 2022;14(12):e16082.

72 Zhou L, He R, Fang P, et al. Hepatitis B virus rigs the cellular metabolome to avoid innate immune recognition. *Nat Commun.* 2021;12(1):98.

73 Zhang W, Wang G, Xu ZG, et al. Lactate is a natural suppressor of RLR signaling by targeting MAVS. *Cell.* 2019;178(1):176–189.e15.

74 Yoshizumi T, Imamura H, Taku T, et al. RLR-mediated antiviral innate immunity requires oxidative phosphorylation activity. *Sci Rep.* 2017;7(1):5379.

75 Chen J, Li Z, Guo J, et al. SARS-CoV-2 nsp5 exhibits stronger catalytic activity and interferon antagonism than its SARS-CoV Ortholog. *J Virol.* 2022;96(8):e0003722.